HOLONOMIC QUANTUM COMPUTATION ON LAGUERRE-GAUSSIAN MODES PROPAGATING IN A HARMONIC DIELECTRIC TRAP

by

Joshua A. Moler

A thesis submitted to the Faculty and the Board of Trustees of the Colorado School of Mines in partial fulfillment of the requirements for the degree of Master of Science (Quantum Engineering).

Golden, Colorado

Date ________________________

Signed: ________________________

Joshua A. Moler

Signed: ________________________

Dr. Mark T. Lusk
Thesis Advisor

Golden, Colorado

Date ________________________

Signed: ________________________

Dr. Frederic Sarazin
Professor and Department Head
Department of Physics

ABSTRACT

Non-Abelian holonomic quantum computing is a method of realizing quantum gates by engineering settings in which cyclic evolution fails to preserve geometric data. Information is encoded as an operator measure of this lack of geometric preservation, and it is not influenced by either the environment or dynamic phase. Non-Abelian holonomic information therefore offers the prospect of being more robust to error than traditional approaches. In this thesis, a comprehensive background is given as an introduction to the field of holonomic quantum computing, and a promising theoretical framework for generating universal honolomic gates is reviewed. This existing framework is then extended by generalizing it to function on arbitrarily large vector spaces, and we prove that the resulting paradigm is sufficient to achieve universal quantum computation. It is then applied to a system of Laguerre-Gaussian modes in a harmonic dielectric trap, and it is shown that this novel optical setting can, in principle, achieve universal quantum computation. The practicality of the implementation is then discussed and compared to other means of realizing quantum computation in the optical regime.

TABLE OF CONTENTS

ABSTRACT . . . iii

LIST OF FIGURES . . . vi

LIST OF TABLES . . . vii

LIST OF SYMBOLS . . . viii

LIST OF ABBREVIATIONS . . . ix

ACKNOWLEDGMENTS . . . x

DEDICATION . . . xi

CHAPTER 1 INTRODUCTION . . . 1

CHAPTER 2 QUANTUM COMPUTING . . . 3

2.1 The Structure of a Qubit . . . 5

2.2 Dealing With Multiple Qubits . . . 6

2.3 A Brief Note on Universality . . . 9

CHAPTER 3 ABELIAN AND NON-ABELIAN HOLONOMIES . . . 10

3.1 General Geometric Phase . . . 12

3.2 Extension to Non-Abelian Holonomies . . . 14

CHAPTER 4 HOLONOMIC QUANTUM LOGIC . . . 18

4.1 Extension to D-Dimensional Holonomic Operators . . . 20

4.2 The Zhu-Wang Scheme for Abelian Geometric Quantum Computation . . . 22

CHAPTER 5 LINEAR OPTICAL QUANTUM COMPUTING . . . 23

5.1 Beam Splitters and Phase Shifters as Unitary Operators . . . 24

5.2 The Reck Scheme . . . 26

5.3 The KLM Protocol . . . 28

CHAPTER 6 GEOMETRIC OPTICAL PHASE AND HOLONOMIC QUANTUM COMPUTING WITH LIGHT . . . 33

6.1 Geometric Phase of an Evolving Plane Wave . . . 33

6.2 The Paraxial Equation 36

6.3 Solutions to the Paraxial Equation 37

6.4 Harmonic Dielectric Trap 38

6.5 Holonomic Gates on Trapped LG Modes 39

6.5.1 Two-qubit encoding with $D = 4$ 41

6.5.2 Physical Implementation and Unresolved Shortcomings 43

CHAPTER 7 CONCLUSIONS AND FUTURE WORK 46

REFERENCES 48

LIST OF FIGURES

Figure 5.1 Depiction of a beam splitter acting on a dual-rail photon state. 25

Figure 5.2 Shows the dual-rail system for two KLM qubits. 29

Figure 5.3 First step to implement a CZ gate for two KLM qubits. A $\theta = \frac{\pi}{4}$ beam splitter is between the 1 rail of the 0 qubit and the 1 rail of the 1 qubit. 30

Figure 5.4 The second step required to implementing a CZ gate for two KLM qubits. An NS gate is inserted on the 1 rail of the 0 qubit and the 1 rail of the 1 qubit. 30

Figure 5.5 The final step to implement a CZ gate for two KLM qubits. A $\theta = \frac{\pi}{4}$ beam splitter is between the 1 rail of the 0 qubit and the 1 rail of the 1 qubit. 31

Figure 5.6 The Non-Linear Sign Shift Gate $|in\rangle$ is the input state, and $|a\rangle$ and $|b\rangle$ are ancilla states with $|a\rangle = |1\rangle$ and $|b\rangle = |0\rangle$. The detectors, D_1 and D_2 are destructive measurement devices which introduce non-linearity. 32

Figure 6.1 (a) Shows geometric phase calculated using Eq. (6.11) compared to numerical data computed using Eq. (3.22). The initial polarization angle, θ, is held fixed while the initial ellipticity, ϕ, is varied from $\frac{\pi}{2}$ to $\frac{3\pi}{2}$. (b) Shows the path taken in polarization space given the initial ellipticity ϕ. 35

LIST OF TABLES

Table 2.1 Shows the possible outcomes of a measurement on two qubits, $|q_0\rangle$ and $|q_1\rangle$. M is decimal value associated with binary result, and ρ_M is the total probability measuring M. 6

Table 6.1 Eigenvectors of $G^{(D)}_{(m,n)}$ with corresponding eigenvalues. 41

Table 6.2 Eigenvectors of $U^{(D)}_{(m,n)}$ with corresponding eigenvalues. 41

Table 6.3 $U^{(4)}_{(m,n)}$ operators corresponding to the universal two qubit gate set, {CNOT, Phase (P), HADAMARD (H)}. 44

Table 6.4 F matrices corresponding to the $U^{(4)}_{(m,n)}$ operators. 45

LIST OF SYMBOLS

A General Control Gate . . . . $C_{i \to j}(U)$

Covariant Tensor Product . . . . $\otimes$

Decimal Value corresponding to a Number Expressed in Binary . . . . $_2ijk\ldots$

Kronecker Delta . . . . $\delta_{i,j}$

Levi-Civita Symbol . . . . $\epsilon_{i,j,k,\ldots}$

The Pauli Spin Matrices . . . . $\{\sigma_1, \sigma_2, \sigma_2\}$

The Set of Integers . . . . $\mathbb{Z}$

The Set of Real Vectors with Dimesion N . . . . $\mathbb{R}^N$

LIST OF ABBREVIATIONS

Bounded-Error Quantum Polynomial Time	BQP
Exact Quantum Polynomial Time	EQP
Group of Special Orthogonal Operators with Dimension N	SO(N)
Group of Special Unitary Operators with Dimension N	SU(N)
Knill, Laflamma, and Milburns.	KLM
Laguerre-Gaussian	LG
Linear Optial Quantum Computing	LOQC
Multi-Mode Fiber	MMF
Noisy Intermediate-Scale Quantum	NISQ
Non-Deterministic Polynomial Time	NP
Non-linear Sign Gate	NS
Orbital Angular Momentum	OAM
Polynomial Time	P
Quantum Merlin-Arthur	QMA
Random Access Memory	RAM
Zhu-Wang	ZW

ACKNOWLEDGMENTS

First and foremost, I would like to thank my research advisor, Dr. Mark Lusk, for taking me under his wing and helping guide my understanding of numerous complex topics. Our enlightening conversations over the last couple years have been both elucidating and enjoyable, and I am grateful for having the opportunity to work with you.

I would also like to thank my committee members including Dr. Jeff Squier, Dr. Zhexuan Gong, and Dr. Mark Siemens, for dedicating their precious time to helping me progress through my education and career. I greatly appreciate their effort and commitment to making this possible.

I also want to express my gratitude to Dr. Eliot Kapit, whose hard work and passion has made the Quantum Engineering program at CSM a reality. Without his dedicated efforts, this thesis may not have been possible.

Finally, I want to thank my close friends and family whose continued encouragement has helped me to reach this point. Perhaps most importantly, I would like to thank Gloria Spedding for sponsoring my education and continuing to provide motivation and support. Without her, I would not be where I am.

For those that shall follow after.

CHAPTER 1
INTRODUCTION

For millions of years, Humans and Hominids have sought to build useful machines that aid us in carrying out certain tasks. The first examples of these machines included simple tools such as wedges and levers. However, as human activity became more complex, so too did the machines we sought to construct. As intellectual thought developed and progressed, the demand for tools grew beyond the need for mechanical advantage. As early as 2700-2300 BCE, the increasing use of arithmetic motivated the invention of the abacus to aid in simple calculations [1]. Approximately 2000 years later, near the first century BCE, was the invention of the device considered by modern researchers to be the world's first computer: the Antikythera mechanism [2]. The device was a form of analog computer thought to have been invented by ancient Greeks and used to track the motion of celestial objects. Fast forward another 2000 years to the early 20th century, and electronic analog computers permeate the world of science and mathematics. Before the year 1900, devices existed capable of analysing harmonic behavior, and by the 1930's, analog differential equation solvers had been developed [3]. In 1958, the first version of a perceptron, the building block for modern artificial neural networks, was implemented on an analog device [4]. The era of analog computers did not last long, however. The first digital computer was constructed in 1939 [5], and with the advent of the transistor in 1948, more generalized digital electronics quickly took off.

The transistor was the final piece of a thousand-year puzzle, allowing for the development of fully universal machines and the start of the digital revolution. Since its invention, silicon technology has continued to progress at a staggering rate, and the power of modern computers continues to increase. However, we are quickly approaching a stage where the physical limitations of silicon transistors may soon put a halt to this progress. As we start to run into the bottlenecks associated with modern computer architectures, some people have begun searching for the next key piece that will allow technological progress to continue. While there are numerous active fields of study focused on the development of more powerful computing devices, one field in particular makes an especially compelling case: quantum computing.

It is widely believed that quantum computers have an intrinsic advantage over their classical counterparts. However, a physical system that convincingly demonstrates this advantage to solve practical problems has yet to be constructed. While a select number of quantum computing architectures have elevated us into the NISQ (Noisy intemediate-scale quantum) era with the potential to become scalable, fault-tolerant machines, there is still an active search for new methods of storing and manipulating quantum information with hopes of achieving a functional quantum advantage. Consistent with the frontier nature of research into optimal quantum computing paradigms, this thesis proposes and analyses a novel method of processing quantum information using Laguerre-Gaussian modes in a harmonic dielectric trap. In this setting, gates would be realized in a purely holonomic manner, making the proposed scheme a theoretical realization of holonomic quantum computing.

This thesis aims not only to propose a new scheme for quantum computing, but also to promote further research and innovation by providing a comprehensive introduction to the field of holonomic optical quantum computing and optical quantum computing. It is structured as follows: Chapter 2 motivates the need for quantum computers from a complexity theory standpoint, and gives a basic introduction to the general theory and mathematics underlying the field. In chapter 3, the concept of geometric phase is introduced and extended to include non-Abelian geometric holonomies in quantum systems. Chapter 4 demonstrates how geometric holonomies can be used to implement robust quantum gates. It then extends an existing framework to one in which universal quantum computing can be achieved on an arbitrarily large Hilbert space. Chapter 5 outlines the current methods used to perform quantum computations in a purely optical setting, and explicitly demonstrates how they are used to carry out operations. Finally, chapter 6 introduces the paraxial equation, which emulates the behavior of a two-dimensional quantum system within a classical optics setting. Next, it presents and demonstrates the proposed method to carry out holonomic quantum computing in the context of the optical modes of a dielectric trap. These chapters serve to answer the primary question that has motivated this research:

Can trapped optical modes be used to carry out universal holonomic quantum computation?

CHAPTER 2

QUANTUM COMPUTING

Digital electronics offer an incredibly powerful solution for carrying out binary logic. In fact, using boolean algebraic techniques and methods, such as a K-map [6], it is fairly simple to design an arbitrary digital circuit to perform any desired binary operation. Furthermore, in combination with memory and timing circuits, digital systems capable of solving any computational problem can be constructed. This begs the question: if classical computers are so powerful, why bother building a quantum computer? Complexity theory offers one possible motivation.

Complexity theory involves the study of computational problems. Specifically, it allows us to quantify the difficulty of a given problem, generally with consideration to the amount of resources required to solve it. It is easy to conflate this field with analysis of algorithms, which deals with the resource requirements of a particular algorithm that can be used to solve a given problem. Complexity theory, on the other hand, considers the difficulty of a problem regardless of the algorithm being employed. In other words, while analysis of algorithms asks "how fast does this algorithm solve this problem," complexity theory asks instead: "how fast can this problem be solved?" The efficiency with which a problem can be solved is generally considered with regards to the worst case, and is expressed in Big-O notation: $O(f(n))$. Here "O" refers to the order of magnitude. In words, given an input of size n, the resource cost has an upper bound on the order of $f(n)$.

Problems are grouped into classes based on how the resource cost varies with the size of the input. Two such classes are P and NP. Problems in P are known to be solvable in polynomial time, meaning that the time required scales as a polynomial of the input size. Using Big-O notation, problems in P run in $O(n^k)$ time, where n is the size of the input and k is an integer. Note that this includes problems with $O(g(n))$ time complexity so long as $g(n)$ is upper-bounded by n^k [7]. P is often considered to be the class of problems that can reasonably be solved by a classical computer.

Unlike problems in P which can be solved in polynomial time, NP problems are such that a particular guess at the solution can be verified in polynomial time. Consider, as an example, the traveling salesman problem: given a set of cities, determine if there exists a closed path which goes through every city exactly once whose distance is less than or equal to some value k. Any given path can easily be checked to see if its total distance is $\leq k$. Yet, determining if any such path exists is much more difficult. It is an open question whether or not P = NP. However, at the time of this writing, many problems in NP do not have solutions that can execute in polynomial time, and many of them are said to be intractable for classical Turing machines. Take, for example, the problem of factoring a non-prime integer into two prime numbers. While prime factorization is a sub-exponential problem [8], it is a still very difficult for computers to solve. In fact, many modern encryption protocols rely on the assumption that it can not be done efficiently.

It is the search for efficient solutions to NP problems that motivates the need for innovations in quantum computing technologies. Quantum computers bring about a new class of problem: BQP, or Bounded-Error Quantum Polynomial Time (among others, such as EQP and QMA). This is the class of problems that can run on a quantum computer in polynomial time with success rates above a given probability threshold. The specific choice of threshold is arbitrary, and as long as it exceeds $\frac{1}{2}$, the class is unchanged. BQP includes all of P, as well as additional problems in NP (and potentially problems outside of NP) which are not yet known to be in P [7]. The famous example of a problem in BQP that may not be in P is prime factorization, mentioned above. This problem was proven to be in BQP in 1995 with the advent of Shor's algorithm (proposed by Peter Shor [9]), the first factoring algorithm with polynomial run-time.

While the potential ability for quantum computers to help solve classical problems that are currently intractable for modern machines is extremely enticing, there is another potential advantage of quantum devices with equally as many (if not more) potential benefits. Large quantum mechanical systems are very difficult for a classical computer to simulate. This is partially due to the vast amount of information encoded within a quantum system. In general, the dimension of the Hilbert space describing n d-level systems grows exponentially as d^n. Thus, describing the full wavefunction of such a system requires an object with d^n elements. Moreover, operators acting on the space require d^{2n} elements to be fully represented. For a system of just 70 interacting two-level systems, storing the wavefunction alone would require enough RAM to hold nearly all of the digital information currently on Earth [10]. This poses quite the bottleneck when it comes to simulating the behavior of large quantum systems. In terms of storing and manipulating quantum information, quantum computers have a distinct (and fairly obvious) advantage over their classical counterparts: they store and manipulate quantum information by default. Thus, they are natural candidates in the search for more efficient methods to carry out simulations of complex quantum systems.

It turns out that, as expected, quantum computers can efficiently simulate quantum mechanical systems [10]. Thus, quantum computers have the potential to revolutionize fields of quantum chemistry, medicine and pharmaceuticals, and many body physics, just to name a few. Moreover, many optimization problems can be reduced to the problem of finding a ground state of a particular Hamiltonian, opening yet another category where quantum computers may prove superior to their classical counterparts.

2.1 The Structure of a Qubit

In order to process information on a quantum system, we first need a container in which we can store the information. For this, we use a single 2-level quantum system called a qubit. We can denote the state of the qubit using bra-ket notation as $|q_0\rangle = \alpha|0\rangle + \beta|1\rangle$, where $|\alpha|^2 + |\beta|^2 = 1$. The set of vectors $|0\rangle$ and $|1\rangle$ form an orthonormal basis called the computational basis. In most cases, this basis is chosen to be $|0\rangle = \begin{pmatrix} 1 \\ 0 \end{pmatrix}$, $|1\rangle = \begin{pmatrix} 0 \\ 1 \end{pmatrix}$, but in general this is not a requirement. Any single-qubit operation can be represented by a rotation on a unit 2-sphere, called the Bloch sphere or Poincare sphere. Usually, the Z axis of the sphere is chosen to represent the $\{|0\rangle, |1\rangle\}$ basis with $|0\rangle$ at the north pole and $|1\rangle$ at the south pole. If this choice is made, convention dictates that $\frac{|0\rangle+|1\rangle}{\sqrt{2}}$ and $\frac{|0\rangle-|1\rangle}{\sqrt{2}}$ lie on the +X and -X axes, respectively. Similarly, $\frac{|0\rangle-i|1\rangle}{\sqrt{2}}$ must be on the +Y axis, and $\frac{|0\rangle+i|1\rangle}{\sqrt{2}}$ must on the -Y axis.

We can now discuss how to rotate the qubit on the Bloch sphere. It is simplest to group rotations in to three categories: rotations about the X axis, $R_x(\theta)$, rotations about the Y axis, $R_y(\theta)$ and rotations about the Z axis, $R_z(\theta)$. We will begin by determining how the qubit state changes under a rotation about each axis, starting with the Z axis. The first thing to note is that if we start with the qubit in the $|0\rangle$ state, then a rotation about the Z axis will never move the state towards the $|1\rangle$ state, and vice versa. We therefore expect this rotation to be diagonal in the Z basis, $\{|0\rangle, |1\rangle\}$. Next, we consider how a qubit in the $\frac{|0\rangle+|1\rangle}{\sqrt{2}}$ state will evolve under this rotation. If the state is rotated by an angle of $\frac{\pi}{2}$, then the final state will be on the +Y axis. Thus, $R_z(\frac{\pi}{2})\left(\frac{|0\rangle+|1\rangle}{\sqrt{2}}\right) = \frac{|0\rangle-i|1\rangle}{\sqrt{2}}$. Following the same line of reasoning, we find that $R_z(\pi)\left(\frac{|0\rangle+|1\rangle}{\sqrt{2}}\right) = \frac{|0\rangle-|1\rangle}{\sqrt{2}}$, and $R_z(\frac{3\pi}{2})\left(\frac{|0\rangle+|1\rangle}{\sqrt{2}}\right) = \frac{|0\rangle+i|1\rangle}{\sqrt{2}}$. From here, it can be deduced that

$$R_z(\theta) \equiv e^{i\frac{\theta}{2}}|0\rangle\langle 0| + e^{-i\frac{\theta}{2}}|1\rangle\langle 1| \tag{2.1}$$

up to an overall phase. Invoking similar arguments for $R_x(\theta)$ and $R_y(\theta)$, we find:

$$R_x(\theta) \equiv \cos\left(\frac{\theta}{2}\right)|0\rangle\langle 0| + i\sin\left(\frac{\theta}{2}\right)|0\rangle\langle 1| + i\sin\left(\frac{\theta}{2}\right)|1\rangle|0\rangle + \cos\left(\frac{\theta}{2}\right)|1\rangle|1\rangle, \tag{2.2}$$

$$R_y(\theta) \equiv \cos\left(\frac{\theta}{2}\right)|0\rangle\langle 0| + \sin\left(\frac{\theta}{2}\right)|0\rangle\langle 1| - \sin\left(\frac{\theta}{2}\right)|1\rangle|0\rangle + \cos\left(\frac{\theta}{2}\right)|1\rangle|1\rangle. \tag{2.3}$$

By keeping in mind the representation of the qubit as a point on a sphere, it is clear that these rotation matrices can produce any unitary operator acting on the qubit. More precisely, products of these operators can produce any operator in SU(2), the group of 2×2 operators with a determinant of 1. Taking the natural log of this set, we find that $\ln(R_j(\theta)) = i\frac{\theta}{2}\sigma_j$, where

$$\sigma_1 = \begin{pmatrix} 0 & 1 \\ 1 & 0 \end{pmatrix} \qquad \sigma_2 = \begin{pmatrix} 0 & -i \\ i & 0 \end{pmatrix} \qquad \sigma_3 = \begin{pmatrix} 1 & 0 \\ 0 & 1 \end{pmatrix} \tag{2.4}$$

are the Pauli spin matrices in the Z basis.

As a brief aside, it is interesting to consider the implications of this analysis from a group theory perspective. What we have done is derived the Lie algebra $\mathfrak{su}(2)$ which generates SU(2). However, we derived it by considering real rotations in three dimensions - the group SO(3). This illustrates the existance of a homomorphism from SU(2) to SO(3). Noting that our 3-D rotations by θ corresponds to an SU(2) rotation by $\frac{\theta}{2}$, we see that this homomorphism is a two-to-one mapping, and SU(2) is a double cover of SO(3). Moreover, this implies that the Lie algebra $\mathfrak{su}(2)$ is isomorphic to $\mathfrak{so}(3)$, which generates SO(3). These algebras are governed by the commutation relations $[t_i, t_j] = \epsilon_{i,j,k} t_k$ where $\epsilon_{i,j,k}$ is the Levi-Civita symbol. This relation may be more easily identified in the context of the $\mathbb{R}^3$ unit vectors, $\vec{X}, \vec{Y}$, and $\vec{Z}$. Specifically, the standard $\mathbb{R}^3$ unit vectors under the cross product form an equivalent Lie algebra, which is why the coordinate frame of the Bloch sphere considered above was chosen in the manner that it was.

2.2 Dealing With Multiple Qubits

While isolated qubits are interesting to consider both physically and mathematically, they are not particularly useful when it comes to performing computations (they would, however, make for a really nice random number generator). In order to make a useful quantum computer, we need instead a set of many qubits with precisely tunable interactions. To see how such a system can be represented, lets start by looking at a two qubit system. Let $|q_0\rangle = \alpha_0 |0\rangle + \beta_0 |1\rangle$ be the state of the first qubit, and $|q_1\rangle = \alpha_1 |0\rangle + \beta_1 |1\rangle$ is the state of the second qubit. If we make a measurement on the system, there are four possible outcomes, detailed in Table 2.1.

Table 2.1 Shows the possible outcomes of a measurement on two qubits, $|q_0\rangle$ and $|q_1\rangle$. M is decimal value associated with binary result, and ρ_M is the total probability measuring M.

M	$\|q_0\rangle$ result	$\|q_0\rangle$ probability	$\|q_1\rangle$ result	$\|q_1\rangle$ probability	ρ_M
0	$\|0\rangle$	α_0	$\|0\rangle$	α_1	$\alpha_0\alpha_1$
1	$\|0\rangle$	α_0	$\|1\rangle$	β_1	$\alpha_0\beta_1$
2	$\|1\rangle$	β_0	$\|0\rangle$	α_1	$\beta_0\alpha_1$
3	$\|1\rangle$	β_0	$\|1\rangle$	β_1	$\beta_0\beta_1$

Following these results, it makes sense to define a new, 4-dimensional vector representing the combined state of both qubits, $|\psi\rangle$, as

$$|\psi\rangle = \rho_0 |0\rangle_0 |0\rangle_1 + \rho_1 |0\rangle_0 |1\rangle_1 + \rho_2 |1\rangle_0 |0\rangle_1 + \rho_3 |1\rangle_0 |1\rangle_1 \tag{2.5}$$
$$= \rho_0 |0_2\rangle + \rho_1 |1_2\rangle + \rho_2 |2_2\rangle + \rho_3 |3_2\rangle . \tag{2.6}$$

In the second line, we have introduced a new basis, $\{|M_2\rangle\}$, which spans the 2-qubit vector space. Conventionally, $\{|M_2\rangle\}$ is structured so that $|i\rangle_0 |j\rangle_1 \equiv |i\rangle_0 \otimes |j\rangle_1$, where $\otimes$ denotes the covariant tensor product. Note that this convention is not required, but is useful for mathematical convenience and consistency, and guarantees that $\{|M_2\rangle\}$ is orthonormal. This is the convention we will use.

In the case of two noninteracting qubits, $\rho_{{}_2ij}$ is always the product of $\langle i|q_0\rangle$ and $\langle j|q_1\rangle$ (where ${}_2ij$ denotes that we are treating ij as the digits of a binary number, and taking the decimal value of that number). However, this is not the case in general. Consider the state:

$$|\Psi^+\rangle = \frac{1}{\sqrt{2}} \left(|1_2\rangle + |2_2\rangle\right) . \tag{2.7}$$

Comparing this to Table 2.1, we see that $\alpha_0\beta_1 = \beta_0\alpha_1 = \frac{1}{\sqrt{2}}$ and $\alpha_0\alpha_1 = \beta_0\beta_1 = 0$. It is not hard to see that this system of equations has no solution. When this is the case, the two qubits are considered to be entangled, and the overall state can not be written as the product of two separate vectors. In the case when this system has a solution, the overall state *can* be written as a product of two separate vectors, thus the qubits are not entangled.

With the representation of a 2-qubit state established, we can now consider how gates act on the $\{M_2\}$ basis. We can consider a unitary operator U_0 acting on $|q_0\rangle$ and a U_1 acting on $|q_1\rangle$. After these operators are applied, the states become: $|q'_j\rangle = \gamma_{0,j} |0\rangle + \gamma_{1,j} |1\rangle$ where $\gamma_{i,j} = (U_j)_{i,0} \alpha_j + (U_j)_{i,1} \beta_j$. Taking the tensor product $|q'_0\rangle |q'_1\rangle$, we get a final 2-qubit state given by

$$|\psi'\rangle = \sum_{i,j} \gamma_{i,0}\gamma_{j,1} |({}_2ij)_2\rangle \tag{2.8}$$
$$= \sum_{i,j} \Big((U_0)_{i,0} (U_1)_{j,0} \rho_0 + (U_0)_{i,0} (U_1)_{j,1} \rho_1 + (U_0)_{i,1} (U_1)_{j,0} \rho_2 + (U_0)_{i,1} (U_1)_{j,1} \rho_3 \Big) |({}_2ij)_2\rangle \tag{2.9}$$
$$= (U_0 \otimes U_1) |({}_2ij)_2\rangle . \tag{2.10}$$

In other words, we have demonstrated that the tensor product satisfies: $(AB) \otimes (CD) = (A \otimes C)(B \otimes D)$ so that operators acting on individual qubits can be represented as a tensor product of the operators acting on the full 2-qubit state. Note that if we only want to apply a gate to one of the qubits, we must still adhere to this structure by applying the tensor product of our desired gate with the identity operator.

Given this tensor product structure for single qubit gates, it is clear that if the input state is separable, the output will be separable as well. Thus, as we should likely expect, multi-qubit operators are required in order to generate entanglement.

Multi-qubit operators can take many forms, but perhaps the most intuitive type is the controlled gate. A controlled gate between the control qubit and the target qubit performs a single qubit gate on the target qubit if and only if the control qubit is in the $|1\rangle$ state. When the qubit i is the control and the qubit j is the target, a general control gate, denoted $C_{i\to j}(U)$, is of the form:

$$C_{i\to j}(U) = \left(|0\rangle_i |0\rangle_j\right)\left(\langle 0|_i \langle 0|_j\right) + \left(|0\rangle_i |1\rangle_j\right)\left(\langle 0|_i \langle 1|_j\right) + U_{0,0}\left(|1\rangle_i |0\rangle_j\right)\left(\langle 1|_i \langle 0|_j\right) + \tag{2.11}$$

$$U_{1,0}\left(|1\rangle_i |1\rangle_j\right)\left(\langle 1|_i \langle 0|_j\right) + U_{0,1}\left(|1\rangle_i |0\rangle_j\right)\left(\langle 1|_i \langle 1|_j\right) + U_{1,1}\left(|1\rangle_i |1\rangle_j\right)\left(\langle 1|_i \langle 1|_j\right). \tag{2.12}$$

Here, to avoid problems with the lack of commutativity of the tensor product on vectors, we have taken the $|q_0\rangle_i |q_1\rangle_j$ notation to mean:

$$|q_0\rangle_i |q_1\rangle_j \equiv \begin{cases} |q_0\rangle_i \otimes |q_1\rangle_j & i < j \\ |q_0\rangle_j \otimes |q_1\rangle_i & j < i \end{cases} \tag{2.13}$$

The ideas of two qubit quantum computing can easily be extended to N qubits. First, we must generalize our computational basis $\{|M_2\rangle\}$ to the 2^N dimensional basis, $\{|M_N\rangle\}$, where

$$|_2(q_0 q_1 \ldots q_{N-2} q_{N-1})_N\rangle = |q_0\rangle_0 |q_1\rangle_1 \ldots |q_{N-2}\rangle_{N-2} |q_{N-1}\rangle_{N-1} \tag{2.14}$$

and q_i can take the value of either 0 or 1. Next, following the result of single qubit gates on two qubit systems, we express the application of N-single qubit gates, O_i, on the overall state, $|\psi\rangle$, as

$$|\psi'\rangle = \left(\bigotimes_{i=0}^{N-1} O_i\right)|\psi\rangle \tag{2.15}$$

where $|\psi'\rangle$ is the output state. This expression can also be generalized to encompass multi-qubit gates that act on subsets of the full set of qubits. Specifically, take $O_{q_i}(n_i)$ to be the operator acting on a set of n_i qubits $q_i, q_i+1, \ldots, q_i+n_i-1$. If there are k such gates, then the total operator acting on $|\psi\rangle$ is given by

$$|\psi'\rangle = \left(\bigotimes_{i=0}^{k-1} O_{q_i}(n_i)\right)|\psi\rangle. \tag{2.16}$$

However, there are two requirements that must be satisfied in order for this expression to correctly represent the operation:

- $\sum_{i=0}^{k-1} n_i = N$

- $q_{i+1} = q_i + n_i \;\; \forall\, i \in \mathbb{Z} \;\; \& \;\; i \in [0, k-1]$.

These guarantee that all qubits are acted on exactly once, and that the tensor product on the operators is done in the correct order.

2.3 A Brief Note on Universality

A universal quantum computer is analogous to a classical Turing machine in that it can be used to construct any quantum circuit. Just as there are countless models of classical computation that are Turing complete, there are many possible ways to achieve universality using quantum gates. Quantum hardware is rarely capable of directly applying arbitrary gates on the system. Thus, it is necessary to be able to efficiently produce arbitrary gates using the gate set that is available to the hardware. One commonly referenced universal gate set consists of three gates: Hadamard (H), Phase (P), and CNOT, shown in matrix form (in the Z basis) in Eq. (2.17).

$$H \equiv \begin{pmatrix} \frac{1}{\sqrt{2}} & \frac{1}{\sqrt{2}} \\ \frac{1}{\sqrt{2}} & -\frac{1}{\sqrt{2}} \end{pmatrix} \qquad P \equiv \begin{pmatrix} e^{i\frac{\theta}{2}} & 0 \\ 0 & e^{-i\frac{\theta}{2}} \end{pmatrix} \qquad CNOT \equiv \begin{pmatrix} 1 & 0 & 0 & 0 \\ 0 & 1 & 0 & 0 \\ 0 & 0 & 0 & 1 \\ 0 & 0 & 1 & 0 \end{pmatrix} \tag{2.17}$$

This set of operators can efficiently produce any special unitary operation[11]. Thus, in order to demonstrate that a different set of gates is universal, it is sufficient to show equivalence to this set.

CHAPTER 3

ABELIAN AND NON-ABELIAN HOLONOMIES

It has long been known that quantum states accumulate a phase as they evolve under the Schrödinger equation, just as light waves accumulate a phase as they propagate under the Maxwell equations. However, it was not until more recently that the existence of another component of phase was discovered. This phase does not depend on the Schrödinger equation. In fact, it does not depend on the system Hamiltonian at all. Instead, this phase, appropriately named the geometric phase, depends exclusively on the geometry of the vector space, and the curve being traversed.

A state, $|n(t)\rangle$ that evolves under the Schrödinger equation will generally accumulate a phase. Perhaps the simplest case of this is the dynamic phase accumulation associated with a stationary state of Hamiltonian, H, as discussed by Zela [12]. Letting $|n\rangle$ and ϵ_n be a pair of solutions to the eigenvalue problem,

$$H\,|n\rangle = \epsilon_n\,|n\rangle\,, \tag{3.1}$$

then $|n(t)\rangle = e^{-i\epsilon_n \frac{t}{\hbar}}\,|n\rangle$ is such a stationary state. The phase accumulation is clearly $\frac{\epsilon_n t}{\hbar}$. Similarly, when the state is a linear combination of stationary states,

$$|\psi\rangle = \sum_n c_n\,|n\rangle\,, \tag{3.2}$$

the linearity of the Schrödinger equation guarantees that

$$|\psi(t)\rangle = \sum_n e^{-\frac{i}{\hbar}t\epsilon_n}\,|n\rangle\,. \tag{3.3}$$

However, this solution assumes H is constant. If we extend this analysis to allow the Hamiltonian to vary with some time-dependent set of parameters, $R_\mu(t)$, then Eq. (3.1) becomes

$$H\left(R_\mu\right)|n(R_\mu)\rangle = \epsilon_n(R_\mu)\,|n(R_\mu)\rangle\,, \tag{3.4}$$

and the time-dependent state is expressed

$$|\psi(R_\mu)\rangle = \sum_n c_n(t)\,|n(R_\mu)\rangle\,. \tag{3.5}$$

Noting that $\partial_t\,|\psi(R_\mu)\rangle = \sum_j \partial_{R_j}\,|\psi(R_\mu)\rangle\,\partial_t R_j$, the time-dependent Schrödinger equation becomes

$$\sum_{n,j}\left(\partial_t c_n(t)\left|n(R_\mu)\right\rangle + c_n(t)\partial_{R_j}\left|n(R_\mu)\right\rangle\partial_t R_j + \frac{i}{\hbar}c_n(t)\epsilon_n(R_\mu)\left|n(R_\mu)\right\rangle\right) = 0. \tag{3.6}$$

Then, if another eigenstate of the Hamiltonian, $|m(R_\mu)\rangle$, is multiplied on the right, Eq. (3.6) becomes

$$\partial_t c_m(t) = \sum_{n,j}\left(ic_n(t)A^j_{m,n}\partial_t R_j\right) - \frac{i}{\hbar}c_m(t)\epsilon_m(R_\mu) \tag{3.7}$$

where $A^j_{m,n} = i\left\langle m(R_\mu)\right|\partial_{R_j}\left|n(R_\mu)\right\rangle$. If we assume the evolution to be adiabatic, then the adiabatic theorem can be used to simplify this expression [12]. For any quantum system with a Hamiltonian that varies slowly in time such that (assuming there is no energy degeneracy) [12],

$$\frac{\left\langle m(R_\mu)\right|\partial_t H\left|n(R_\mu)\right\rangle}{E_n(R_\mu) - E_m(R_\mu)} \approx 0 \quad \forall \quad m \neq n, \tag{3.8}$$

then the system will remain in its instantaneous eigenstate. Invoking this assumption on $A^j_{m,n}$ implies that $A^j_{m,n} \approx A^j_{m,n}\delta_{m,n}$, and Eq. (3.7) becomes

$$\partial_t c_m(t) = i\left(A^j_{m,m}\partial_t R_j - \frac{1}{\hbar}\epsilon_m(R_\mu)\right)c_m(t) \tag{3.9}$$

where the summation over j is implied and $\sum_j$ has been left out for simplicity. The differential equation in Eq. (3.9) has a well-known solution:

$$c_m(t) = e^{i\gamma_m}e^{i\phi_m}c_m(t_0), \tag{3.10}$$

where ϕ_m is the dynamic phase given by

$$\phi_m = -\frac{1}{\hbar}\int_{t_0}^{t}\epsilon_m(R_\mu(t'))dt' \tag{3.11}$$

and γ_m is the geometric phase (often called the Berry phase):

$$\gamma_m = \int_{t_0}^{t}A^j_{m,m}\partial_{t'}R_j(t')dt' = \int_C A^j_{m,m}dR_j. \tag{3.12}$$

Here, C is the curve traversed through the parameter space with endpoints $R_\mu(t_0)$ and $R_\mu(t)$.

In general, while the dynamic phase depends on the energy of the state and the total time of the evolution, the geometric phase is an Abelian holonomy resulting from the parallel transport of the state vector over a curved manifold, thus it depends on the geometry of the evolution through some parameter space rather than the total time. This is evident when looking at Eq. (3.12), which is a special case of Eq.

(3.22) corresponding to adiabatic evolution. In fact, for two level systems it can be shown that the geometric phase reduces to half of the solid angle enclosed by the path of the evolution on the Bloch sphere [12]. This is analogous to the classic example of a pendulum on a globe:

Suppose you are standing at the North Pole, holding a pendulum that you have set in motion so that it swings along the prime meridian. Then, if you slowly turn in a circle, the pendulum will continue swinging along the prime meridian the entire time, so long as your motion is slow enough. Now, say you walk straight straight down the prime meridian to the equator, turn right, and head to 90° west. Assume that the whole time you are moving, you do so slowly enough as to not interfere with the motion of the pendulum. Finally, you walk back up the to North Pole. Following this process, the pendulum will no longer be swinging along the prime meridian. In fact, it will have rotated by $\frac{\pi}{2}$, equivalent to the solid angle you enclosed when covering the quarter hemisphere of the globe.

3.1 General Geometric Phase

While geometric phases were first considered in the context of adiabatic evolution, it was quickly shown by Aharonov and Anandan [13] that geometric phase can also be quantified without the need for this approximation. In order to demonstrate this, we begin with a new state $|\psi(t)\rangle$ that evolves under a Hamiltonian, $H(t)$, according to the time-dependent Schrödinger equation,

$$H(t)\,|\psi(t)\rangle = i\hbar\partial_t\,|\psi(t)\rangle\,. \tag{3.13}$$

At some time, t_f, assume that $|\psi(t_f)\rangle = e^{i\delta}\,|\psi(t_0)\rangle$. Next, define a second state, $|\phi(t)\rangle = e^{-if(t)}\,|\psi(t)\rangle$. Substituting this into Eq. (3.13) gives

$$\frac{1}{\hbar}\,\langle\psi(t)|\,H(t)\,|\psi(t)\rangle - i\,\langle\phi(t)|\,\partial_t\,|\phi(t)\rangle + \partial_t f(t) = 0 \tag{3.14}$$

$$\implies f(t_f) - f(t_0) = -\frac{1}{\hbar}\int_{t_0}^{t_f}\langle\psi(t)|\,H(t)\,|\psi(t)\rangle\,dt + i\int_{t_0}^{t_f}\langle\phi(t)|\,\partial_t\,|\phi(t)\rangle\,dt. \tag{3.15}$$

If we require $|\phi(t_f)\rangle = |\phi(t_0)\rangle$ so that $f(t_f) - f(t_0) = \delta$, then the total phase again has two contributions, the dynamic phase and the geometric phase. The dynamic component, ϕ, is equivalent to the adiabatic case in Eq. (3.11):

$$\phi = -\int_{t_0}^{t_f}\langle\psi(t)|\,H(t)\,|\psi(t)\rangle\,dt = -\int_{t_0}^{t_f}\epsilon(t)dt. \tag{3.16}$$

The geometric phase is now

$$\gamma = i \int_{t_0}^{t_f} \langle \phi(t) | \, \partial_t \, | \phi(t) \rangle \, dt. \tag{3.17}$$

By considering a second state evolving in the Hilbert space, $|\phi(t)\rangle$, we were able to acquire a geometric phase term without invoking the adiabatic approximation. In fact, the geometric phase can be generalized even further to include both non-unitary and non-cyclic evolutions as well [14]. To construct a completely general expression for the geometric phase, we note that there are always two contributions to the total phase: the dynamic phase, ϕ, and the geometric phase, γ. The total phase, δ, is simply the sum of these two components,

$$\delta = \phi + \gamma \tag{3.18}$$

To characterize γ, it is first necessary to quantify both δ and ϕ. δ is the simplest of the two, and can be thought of as the phase difference between the initial and final states. Given an initial state, $|\psi_i\rangle \equiv e^{-i\alpha_i} |\phi_i\rangle$, which evolves to the final state, $|\psi_f\rangle \equiv e^{-i\alpha_f} |\phi_i\rangle$, the total phase between the two states is simply $\alpha_f - \alpha_i$. For general $|\psi_i\rangle$ and $|\psi_f\rangle$, this is expressed as [12]

$$\delta \equiv \arg\left(\langle \psi_i | \psi_f \rangle\right). \tag{3.19}$$

To acquire the dynamic phase, we look to Eq. (3.11) and Eq. (3.16), and express the energy as the expectation value of the Hamiltonian:

$$\phi \equiv \arg\left(e^{-\frac{i}{\hbar}\int_{t_i}^{t_f} \langle \psi(t)|H(t)|\psi(t)\rangle dt} \right) \tag{3.20}$$

$$= \mathrm{Im}\left(\int_{t_i}^{t_f} \langle \psi(t) | \dot{\psi}(t) \rangle \, dt \right) \tag{3.21}$$

where Eq. (3.21) is acquired from Eq. (3.20) by applying the time-dependant Schrodinger equation, and noting that $\langle \phi(s)|\dot{\phi}(s)\rangle = i\mathrm{Im}(\langle \phi(s)|\dot{\phi}(s)\rangle)$. Combining Eq. (3.18), Eq. (3.19), and Eq. (3.21) gives the general form of the geometric phase[12]:

$$\gamma \equiv \arg(\langle \psi(s_i) | \psi(s_f) \rangle) - \mathrm{Im}\left(\int_{s_i}^{s_f} \langle \psi(s) | \dot{\psi}(s) \rangle \, ds \right). \tag{3.22}$$

Note that while both the total phase and the dynamic phase can be removed by a particular choice of gauge, the geometric phase is gauge invariant under the local phase transformation $|\psi\rangle \to |\psi'\rangle = e^{i\alpha(s)} |\psi\rangle$:

$$
\begin{aligned}
\gamma \to \gamma' &= \arg(e^{-i\alpha(s_i)} e^{i\alpha(s_f)} \langle \psi(s_i) | \psi(s_f) \rangle) \\
&- \mathrm{Im}\left(\int_{s_i}^{s_f} e^{-i\alpha(s)} \langle \psi(s) | \, \partial_s \left(e^{i\alpha(s)} | \psi(s) \rangle \right) ds \right)
\end{aligned} \tag{3.23}
$$

$$
\begin{aligned}
&= \alpha(s_f) - \alpha(s_i) + \arg\left(\langle \psi(s_i) | \psi(s_f) \rangle \right) \\
&- \mathrm{Im}\left(\int_{s_i}^{s_f} \langle \psi(s) | \dot{\psi}(s) \rangle \, ds - \int_{s_i}^{s_f} \alpha(s) ds \right)
\end{aligned} \tag{3.24}
$$

$$
= \arg(\langle \psi(s_i) | \psi(s_f) \rangle) - \mathrm{Im}\left(\int_{s_i}^{s_f} \langle \psi(s) | \dot{\psi}(s) \rangle \, ds \right). \tag{3.25}
$$

3.2 Extension to Non-Abelian Holonomies

As briefly mentioned above, the geometric phase is an example of an Abelian holonomy. That said, it is reasonable to ask what this means, and why it is the case. In general, the holonomy resulting from the evolution of a quantum system can be represented as an operator acting on the Hilbert space. If we consider the general state $|\psi\rangle$ in Eq. (3.2), the operator representing the accumulation of a geometric phase, γ, is given by

$$
O(\gamma) = \sum_n e^{i\gamma_n} |n\rangle \langle n| \,. \tag{3.26}
$$

If we take γ_n to be a free set of parameters, then the resulting set of possible operators forms an Abelian subgroup, $H_{g.p.}(N)$, of $U(N)$ (for an N dimensional Hilbert space). This is the holonomy group characterizing the geometric phase. It is straightforward to verify that this group is Abelian by calculating the commutator of two arbitrary group elements:

$$
\begin{aligned}
[O(\alpha), O(\beta)] &= \sum_n \sum_m \left(e^{i\alpha_n} e^{i\beta_m} |n\rangle \langle n| \, |m\rangle \langle m| - e^{i\beta_m} e^{i\alpha_n} |m\rangle \langle m| \, |n\rangle \langle n| \right) \\
&= \sum_n \left[e^{i\alpha_n}, e^{i\beta_n} \right] |n\rangle \langle n| \,.
\end{aligned} \tag{3.27}
$$

Because the phases α_n and β_n are scalar valued, $e^{i\alpha_n}$ and $e^{i\beta_n}$ are both elements of $U(1)$. Therefore, their commutator is zero, and the value of $[O(\alpha), O(\beta)]$ is also zero. Since the elements of $H_{g.p.}(N)$ commute, we say that $H_{g.p.}(N)$ is an Abelian group.

It is also possible to quantify non-Abelian holonomies resulting from quantum evolutions. As with the case of geometric phase, this was first realized in the adiabatic setting [15]. To see how this can be done, recall the simplification of Eq. (3.7) to Eq. (3.9) by invoking the adiabatic approximation, Eq. (3.8). The form of the adiabatic approximation required the assumption that the Hamiltonian was non-degenerate. In other words, it was assumed that $E_m \neq E_n \; \forall \; m \neq n$. If we relax this assumption, the adiabatic approximation can still be invoked, only the form becomes

$$\frac{\langle m(R_\mu)| \partial_t H |n(R_\mu)\rangle}{E_n(R_\mu) - E_m(R_\mu)} \approx 0 \quad \forall \quad E_m(R_\mu) \neq E_n(R_\mu). \tag{3.28}$$

This is nearly identical to Eq. (3.8) but has now been extended to allow degenerate energy levels. In the former case, $\sum_n A^j_{m,n}$ reduced to a single term, $A^j_{m,m}$. However, if some subspace, $\mathbb{S}_0$, of the Hilbert space satisfies $\langle k| H |k\rangle = E_m(R_\mu) \; \forall \; |k\rangle \in \mathbb{S}_0$, $\sum_n A^j_{m,n}$ instead reduces to $\sum_{|k\rangle \in \mathbb{S}_0} A^j_{m,k}$, and Eq. (3.9) becomes

$$\partial_t c_m(t) = i \left(A^j_{m,k} \partial_t R_j - \frac{1}{\hbar} \epsilon_m(R_\mu) \delta_{m,k} \right) c_k(t). \tag{3.29}$$

The implied sum over k is once again restricted to $\mathbb{S}_0$. As before, $\vec{c}(t)$ evolves in time under the evolution operator, $e^{i\Gamma} e^{i\Phi}$, where the dynamic phase operator, Φ, is given by

$$\Phi_{m,k} = \frac{1}{\hbar} \int_{t_0}^{t} \epsilon_m(R_\mu(t')) \delta_{m,k} dt'. \tag{3.30}$$

Likewise, the operator, Γ, is the non-Abelian Wilczek-Zee Holonomy[15], given by

$$\Gamma_{m,k} = \int_{t_0}^{t} A^j_{m,k} \partial_t R_j(t') dt' = \int_C A^j_{m,k} dR_j. \tag{3.31}$$

Here,

$$A^j_{m,k} = i \langle m(R_\mu)| \partial_{R_j} |k(R_\mu)\rangle \,, \qquad |m\rangle \,, |k\rangle \in \mathbb{S}_0. \tag{3.32}$$

This holonomy is a unitary operator that transforms states within the degenerate subspace. However, it still relies on the adiabatic approximation, and this restricts the allowable speed of evolution. That can become an issue, particular for applications in quantum computing because of the short decoherence times of many qubit architectures. Thus, it would be ideal to generalize the ideas to non-Abelian evolutions, and this will now be carried out.

Following the work of Anandan [16] with additional insights provided by Bohm et al. [17], consider an arbitrary N-dimensional subspace, $\mathbb{S}$, of the Hilbert space. Note that unlike $\mathbb{S}_0$ above, we will not yet restrict $\mathbb{S}$ to a particular subspace. Let $S_\psi \equiv \{|\psi_m(t)\rangle \,|, \; m \in \mathbb{Z}\,, \;\; m \in [0, N-1]$, be an orthonormal basis for $\mathbb{S}$ that evolves under H according to the time-dependent Schrödinger equation. Let $S_\phi \equiv \{|\phi_m(t)\rangle \,|, \; m \in \mathbb{Z}, \, m \in [0, N-1]\}$ be an orthonormal basis for $\mathbb{S}$ that does not satisfy the Schrödinger equation for H. Since the two basis sets are both orthonormal and cover the same space, we can express $|\psi_m\rangle$ in terms basis vectors of S_ϕ as

$$|\psi_m(t)\rangle = F_{k,m}(t)\,|\phi_k(t)\rangle\,. \tag{3.33}$$

Here $F(t)$ is a unitary operator, and $|\psi_m(t)\rangle$ satisfies the Schrödinger equation. This knowledge and Eq. (3.33) can be used to build an equation for $F_{k,m}(t)$:

$$i\hbar\partial_t\left(F_{k,m}(t)\,|\phi_k(t)\rangle\right) = H(F_{k,m}(t)\,|\phi_k(t)\rangle). \tag{3.34}$$

Taking the derivative on the right hand side and multiplying both sides of the equation by $\langle\phi_c(t)|$ results in a Schrödinger equation for $F_{k,m}(t)$:

$$\partial_t F_{c,m}(t) = i(A_{c,k}(t) - K_{c,k}(t))F_{k,m}(t). \tag{3.35}$$

Here $A_{c,k}(t) = i\,\langle\phi_c(t)|\partial_t\phi_k(t)\rangle$ is the geometric component of the evolution analogous to the Wilczek-Zee Holonomy, and $K_{c,k}(t) = \frac{1}{\hbar}\,\langle\phi_c(t)|\,H\,|\phi_k(t)\rangle$ characterizes the dynamics of the system. This can be formally integrated to give

$$F(t) = \mathcal{T}e^{i\int_{t_0}^{t} dt\left(A(t)-K(t)\right)}. \tag{3.36}$$

where $\mathcal{T}$ is the Dyson time-ordering operator. Note that if $t = t_0$, then $F(t)$ becomes the identity matrix and $|\psi_m(t_0)\rangle = \delta_{k,m}\,|\phi_k(t_0)\rangle = |\phi_m(t_0)\rangle$. We must therefore require that for every $|\psi_m(t)\rangle \in S_\psi$, there exists a vector in S_ϕ, call it $|\phi_m(t)\rangle$, so that $|\psi_m(t_0)\rangle = |\phi_m(t_0)\rangle$. With this requirement, $|\psi_m(t)\rangle$ can be expressed as a time-evolution operator acting on $|\psi_m(t_0)\rangle$:

$$|\psi_m(t)\rangle = F_{k,m}(t)\,|\phi_k(t)\rangle\,\langle\phi_m(t_0)|\psi_m(t_0)\rangle\,. \tag{3.37}$$

As an additional constraint, it can be useful to force S_ϕ to be periodic so that $|\phi_k(t_0)\rangle = |\phi_k(t_f)\rangle\ \forall$ $|\phi\rangle \in S_\phi$ for some t_0 and t_f. Then, the final time-evolution operator on $S_\psi(t_0)$, $F(t_f)$, becomes

$$F(t_f) \equiv F_{k,m}(t_f)\,|\phi_k(t_0)\rangle\,\langle\phi_m(t_0)| = F_{k,m}(t_f)\,|\psi_k(t_0)\rangle\,\langle\psi_m(t_0)|\,, \tag{3.38}$$

so that $|\psi_j(t_f)\rangle = F(t_f)\,|\psi_j(t_0)\rangle$. The unitary operator, $F(t_f)$, represents the holonomy for non-Abelian, nonadiabatic, cyclic processes.

It is also insightful to look in depth at the contributions to the evolution operator, $A(t)$ and $K(t)$. For example, given that the choice of S_ϕ is seemingly arbitrary up to the prescribed constraints, it is natural to ask what happens if a different basis is selected. Let $|\phi'_m(t)\rangle = \Omega_{b,m}(t)\,|\phi_b(t)\rangle$. Then $K(t)$ transforms to $K'(t)$ as

$$K'_{m,k}(t) = \langle \phi'_m(t)| H |\phi'_k(t)\rangle \tag{3.39}$$
$$= \langle \phi_b t| \Omega^*_{b,m} H \Omega_{a,k} |\phi_a(t)\rangle \tag{3.40}$$
$$= \left(\Omega^\dagger\right)_{m,b} \langle \phi_b(t)| H |\phi_a(t)\rangle \Omega_{a,k} \tag{3.41}$$
$$\implies K'(t) = \Omega^\dagger K \Omega, \tag{3.42}$$

while $A(t)$ transforms to $A'(t)$ as

$$A'_{m,k}(t) = i \langle \phi'_m(t)| \partial_t |\phi'_k(t)\rangle \tag{3.43}$$
$$= i\Omega^*_{b,m} \langle \phi_b(t)|\phi_a(t)\rangle \partial_t \Omega_{a,k} + i\Omega^*_{b,m} \langle \phi_b(t)| \partial_t |\phi_a(t)\rangle \Omega_{a,k} \tag{3.44}$$
$$= i \left(\Omega^\dagger\right)_{m,a} \partial_t \Omega_{a,d} + \left(\Omega^\dagger\right)_{m,b} A_{b,a} \Omega_{a,k} \tag{3.45}$$
$$\implies A'(t) = i\Omega^\dagger \partial_t \Omega + \Omega^\dagger A \Omega. \tag{3.46}$$

Under a change of basis, $A(t)$ transforms as a connection 1-form, thus it is a true gauge potential [16]. One notable feature about this transformation rule is that a zero-valued potential in one basis can produce a non-zero potential in a different basis. K, on the other hand, does not have this property. If K is zero for any S_ϕ, then it is zero for all S_ϕ. This is critical when considering that K is the only appearance of H in $U(t)$. Specifically, If $K = 0$, then the evolution of $|\psi(t)\rangle$ is purely geometric.

The key feature which distinguishes non-Abelian holonomies from their Abelian counterpart, the geometric phase, is the existence of off-diagonal components in the holonomy operator. Specifically, unlike in the Abelian case, the operators in the non-Abelian case can not be simultaneously diagonalized. While on the surface this seems like a simple generalization, it has significant impacts on both algebraic structure and potential applications. Specifically, the holonomy operators in the non-Abelian case are elements of a non-Abelian group, $H(N) \leq U(N)$ [18]. Unlike $H_{g.p}(N)$, which has elements that are only capable of modifying the relative phases of the basis vectors, $H(N)$ has elements which are also capable of modifying the relative amplitudes of the basis vectors. These distinct operations can be understood in terms of a two level system on a Bloch sphere. In this setting, $H_{g.p.}(N)$ induces rotations about the Z axis. These rotations are not sufficient for applications such as quantum computing because the are incapable of altering the "latitude" of the state, which is necessary for full control of the system. $H(N)$, on the other hand, induces rotations in more than one degree of freedom. This means that both the "latitude" and "longitude" can be controlled, making universal operations possible.

CHAPTER 4

HOLONOMIC QUANTUM LOGIC

Many popular quantum computing architectures suffer from high noise and decoherence rates[19]. While Noisy Intermediate-Scale Quantum (NISQ) computers are generally sufficient to demonstrate error-resilient circuits including optimization protocols, quantum simulations, and quantum machine learning algorithms, they are not capable of performing more delicate operations at a useful scale. For example, widely sought after algorithms such as amplitude amplification (Grover's search), quantum Fourier transforms, and the coveted Shor's algorithm are all single-error fragile. In other words, their output elicits chaotic deviations in response to small perturbations throughout the circuit.

To develop more useful quantum computing devices, a necessary prerequisite is the mitigation of errors. One promising approach is the use of passive error correcting codes which simulate a Hamiltonian of topological quantum order [19]. These codes seek to emulate anyonic behavior, in which quantum information can be stored nonlocally and is therefore resilient to local perturbations in the system [20]. However, this approach comes with some notable drawbacks, one of which being its high resource cost [19]. In fact, some implementations have overheads on the order of 100 - 1000 physical qubits per logical qubit to achieve fault-tolerance [21]. Moreover, sufficiently aggressive error sources can undermine the functionality of error correcting codes. In superconducting systems, for example, cosmic rays induce physical errors significant enough to prevent error correction from working properly [22, 23].

While quantum error correction is an exciting facet of the current research frontier, another strategy is to attempt to design qubits with less sensitivity to environmental noise. Unfortunately, such an endeavor is easier said than done. One front being explored is the production of physical systems with topological order, bypassing the need to simulate them with large qubit arrays. This effort underlies topological quantum computing, in which physical quasiparticle excitations (anyons) are manipulated to store quantum information nonlocally [20]. Although this is a compelling and elegant approach to achieve fault-tolerance, the existence of the requisite non-Abelian anyons has yet to be demonstrated.

There is also a middle ground between topological quantum computing and current paradigms that is experimentally tractable. Holonomic quantum computing seeks to exploit the geometry of a quantum system to achieve evolutions with increased resilience to noise than traditional methods. Unlike topological quantum computing, which relies on exotic quantum excitations that have not yet been discovered, holonomic quantum computing can be achieved using systems that already exist in laboratories. General implementations rely on the ability to realize Hamiltonians which suppress the dynamic evolution of some subspace S, as described in section 3.2.

An example of such a Hamiltonian can be found in trapped ion systems, proposed and analyzed by Sjöqvist [24]. Consider a three-level ion with stationary states states denoted by $|0\rangle, |1\rangle$, and $|e\rangle$. By driving the $|0\rangle \to |e\rangle$ and $|1\rangle \to |e\rangle$ transitions independently using tuned laser pulses, the Hamiltonian can be expressed in the form [24]

$$H(t) = \Omega(t)(\omega_0 |e\rangle \langle 0| + \omega_1 |e\rangle \langle 1| + \text{h.c.}). \tag{4.1}$$

Here $\Omega(t)$ is the Rabi frequency, and the frequency parameters are constrained so that $|\omega_0|^2 + |\omega_1|^2 = 1$. The set S_ψ is chosen to be $\{|d\rangle, |b\rangle\}$ where $|d\rangle = -\omega_1 |0\rangle + \omega_0 |1\rangle$ is referred to as the dark state, and $|b\rangle = \omega_0^* |0\rangle + \omega_1^* |1\rangle$ is referred to as the bright state. The set S_ϕ is chosen to be $\{|\phi_0(t)\rangle, |\phi_1(t)\rangle\}$, given by

$$\begin{aligned} |\phi_0(t)\rangle &= |d\rangle \\ |\phi_1(t)\rangle &= e^{i\delta(t)}(\cos(\delta(t))\,|b\rangle - i\sin(\delta(t))\,|e\rangle), \end{aligned} \tag{4.2}$$

where $\delta(t) = \int_{t_0}^{t} \Omega(t')dt'$. The requirement that $|\phi_m(t_f)\rangle = |\phi_m(t_0)\rangle$ forces $\delta(t_f) = N\pi \implies \int_{t_0}^{t_f} \Omega(t) = N\pi$ for $N \in \mathbb{Z}$. It is straightforward to show through explicit calculation that $K_{m,k} = \langle \phi_m(t)| H(t) |\phi_k(t)\rangle = 0$, thus the evolution of this system will be purely geometric under A. The only non-zero element of A is $A_{1,1} = -\partial_t \delta(t)$. Thus, $F(t_f)_{1,1} = e^{-\int_{t_0}^{t_f} \Omega(t)dt} = e^{-Ni\pi} = 1 - 2(N\text{mod}2)$. Noting additionally that $F(t_f)_{0,0} = e^0 = 1$, it is clear that $F(t_f) = \sigma_3$ for odd N, and $F(t_f) = \sigma_0$ for even N. Because evolution under σ_0 is trivial, we restrict N to odd values so that $U(t_f) = F(t_f)_{k,m} |\phi_k(t_0)\rangle \langle \phi_m(t_0)|$ becomes

$$U(t_f) = (|\omega_1|^2 - |\omega_0|^2)\,|0\rangle \langle 0| - 2\omega_1\omega_0^* |0\rangle \langle 1| - 2\omega_0\omega_1^* |1\rangle \langle 0| + (|\omega_0|^2 - |\omega_1|^2)\,|1\rangle \langle 1|\,. \tag{4.3}$$

Letting ω_1 and ω_2 be arbitrary complex numbers (keeping normalization in mind, of course), $U(t)$ is a universal single qubit gate in the computational basis $\{|0\rangle, |1\rangle\}$.

While the unitary operator of Eq. 4.3 may be either Abelian or non-Abelian, the delineation in character is made clear by the following alternate representation of the component of U that acts on the degenerate subspace [24]:

$$[U(t_f)] = \vec{n} \cdot \vec{\sigma}, \tag{4.4}$$

where $\vec{n}$ is a unit vector described with spherical coordinates in the $\{|\phi_1(0)\rangle, |\phi_2(0)\rangle\}$ basis and $\vec{\sigma}$ is the Pauli vector:

$$
\begin{aligned}
\vec{n} &= \{\cos\phi_\omega \sin\theta_\omega, \sin\phi_\omega \sin\theta_\omega, \cos\theta_\omega\} \\
\omega_0 &= e^{i\phi_\omega} \sin\theta_\omega/2, \quad \omega_1 = -\cos\theta_\omega/2 \\
\vec{\sigma} &= \{[\sigma_x], [\sigma_y], [\sigma_z]\} \qquad (4.5)
\end{aligned}
$$

This is the SU(2) analog to Euler's Rotation Theorem for SO(3) in which any set of rotations about fixed axes are shown to be equivalent to one rotation about a single axes. Each operator, by itself, therefore corresponds to motion on a particular circular arc in SU(2). A sequence of operations, each tracing an arc, can be constructed so that a closed curvilinear polygon is created. The solid angle enclosed is equal to twice the geometric phase. However, if a sequence of operators is applied with a full rotation about their respective unit normals, then a geometric phase is generated for each closed loop, and the order in which the operations are carried out does not change the total geometric phase accumulated. The sequence of such operations is therefore Abelian.

Non-Abelian behavior is elicited when two operators are sequentially applied with a 180° rotation about their respective unit normals, $\vec{n}$. The degenerate subspace associated with the Hamiltonian of Eq. 4.1 will then flip in each operation. The final orientations of an orthonormal basis of the degenerate space will then depend on the order in which the operations were applied–i.e. the operators produce a non-Abelian evolution of vectors in the degenerate subspace.

4.1 Extension to D-Dimensional Holonomic Operators

We now propose a generalization of the above framework to allow universal logic operations on a vector space of arbitrary dimension. Using the structure associated with this example, it is possible to formulate a universal gate set acting on a D-dimensional subspace, S_D, of a $(D+1)$-dimensional Hilbert space. Consider the set $G^{(D)}$, consisting of $\binom{D}{2}$ $(D+1)$-dimensional Hamiltonian operators. Let $M^{(D)}$ contain the integers $[0, D-2]$ and $N_m^{(D)}$ contain the integers $[m, D-1]$. We can then define $G_{(m,n)}^{(D)}$ as the Hamiltonian given by

$$
G_{(m,n)}^{(D)} \equiv \Omega_{(m,n)}(t)\left(\omega_m \left|e\right\rangle \left\langle m\right| + \omega_n \left|e\right\rangle \left\langle n\right| + H.C.\right), \quad m \in M^{(D)} \;\;\&\;\; n \in N_m^{(D)}. \qquad (4.6)
$$

For each Hamiltonian, we identify the "dark state," $|d_{(m,n)}\rangle \equiv -\omega_n |m\rangle + \omega_m |n\rangle$, and the "bright state," $|b_{(m,n)}\rangle \equiv \omega_m^* |m\rangle + \omega_n^* |n\rangle$. Just as before, we choose $s_{\psi,(m,n)}$ to be the set $\{|d_{(m,n)}\rangle, |b_{(m,n)}\rangle\}$, and s_ϕ to be $\{|\phi_{0,(m,n)}(t)\rangle, |\phi_{1,(m,n)}(t)\rangle\}$ with

$$
|\phi_{0,(m,n)}(t)\rangle = |d_{(m,n)}\rangle\,, \qquad (4.7)
$$

$$
|\phi_{1,(m,n)}(t)\rangle = e^{i\delta_{(m,n)}(t)}(\cos(\delta_{(m,n)}(t))\,|b_{(m,n)}\rangle - i\sin(\delta_{(m,n)}(t))\,|e\rangle). \qquad (4.8)
$$

Again, $\delta_{(m,n)}(t) = \int_{t_0}^{t} \Omega_{(m,n)}(t')dt'$ and $\delta_{(m,n)}(t_f) = N\pi$ for some odd N. As expected, this evolution is purely geometric because $K_{j,k,(m,n)} = \langle\phi_{j,(m,n)}| G^{(D)}_{(m,n)} |\phi_{k,(m,n)}\rangle = 0$. Similarly, the only non-zero element of $A_{(m,n)}$ is $A_{1,1,(m,n)} = -\partial_t \delta_{(m,n)}(t)$, and $F_{(m,n)}(t_f) = \sigma_3$. It then follows that the final evolution of the $\{|m\rangle, |n\rangle\}$ subspace is given by

$$U_{(m,n)}(t_f) = \left(|\omega_n|^2 - |\omega_m|^2\right)|m\rangle\langle m| - 2\omega_n\omega_m^*|m\rangle\langle n| - 2\omega_m\omega_n^*|n\rangle\langle m| + \left(|\omega_m|^2 - |\omega_n|^2\right)|n\rangle\langle n|. \tag{4.9}$$

Critically, the evolution of S_D is fully restricted to the $\{|m\rangle, |n\rangle\}$ subspace. In fact, it can be shown that the evolution of the entire Hilbert space under $G^{(D)}_{(m,n)}$, given by $U^{(D)}_{(m,n)}(t_f) = e^{-i\pi G^{(D)}_{(m,n)}}$, becomes

$$U^{(D)}_{(m,n)}(t_f) = U_{(m,n)}(t_f) + \left(\sum_{k\notin\{m,n\}} |k\rangle\langle k|\right) - |e\rangle\langle e| \tag{4.10}$$

so that all states in S_D evolve under the identity except for $|m\rangle$ and $|n\rangle$.

$U^{(D)}(t_f)$ is dense in $U(D)$, the group of D-dimensional unitary operators. In other words, it forms a universal gate set on a D-dimensional Hilbert space. To see how this is true, note that operation of $U^{(D)}_{(m,n)}(t_f)$ is exactly equivalent to that of a beam splitter acting on the m and n rails of a D rail system. The universality of these operators along with arbitrary phase gates is proven in Chapter 5.2. It is therefore sufficient to demonstrate that a phase gate can be produced in this context.

Consider the sequential application of $U^{(D)}_{(m,n)}(t_f)$ and $U^{(D)}_{(i,j)}(t_f)$ where $|i\rangle = |m\rangle$ and $|j\rangle = |n\rangle$, which produces

$$U^{(D)}_{(m,n)}(t_f) \cdot U^{(D)}_{(i,j)}(t_f) = U_{(m,n)}(t_f) \cdot U_{(i,j)}(t_f) + \left(\sum_{k\notin\{m,n\}} |k\rangle\langle k|\right) - |e\rangle\langle e|, \tag{4.11}$$

where

$$\begin{aligned} U_{(m,n)}(t_f) \cdot U_{(i,j)}(t_f) = & \\ & \left[\left(|\omega_n|^2 - |\omega_m|^2\right)\left(|\omega_j|^2 - |\omega_i|^2\right) + 4\omega_n\omega_i\omega_m^*\omega_j^*\right]|m\rangle\langle m| \\ & -2\left[\omega_m\omega_n^*\left(|\omega_j|^2 - |\omega_i|^2\right) + \omega_i\omega_j^*\left(|\omega_m|^2 - |\omega_n|^2\right)\right]|n\rangle\langle m| \\ & -2\left[\omega_n\omega_m^*\left(|\omega_i|^2 - |\omega_j|^2\right) + \omega_j\omega_i^*\left(|\omega_n|^2 - |\omega_m|^2\right)\right]|m\rangle\langle n| \\ & +\left[\left(|\omega_m|^2 - |\omega_n|^2\right)\left(|\omega_i|^2 - |\omega_j|^2\right) + 4\omega_m\omega_j\omega_n^*\omega_i^*\right]|n\rangle\langle n|. \end{aligned} \tag{4.12}$$

Critically, this produces phase terms on the diagonal. In the simple case where $\left(|\omega_n|^2 - |\omega_m|^2\right) = \left(|\omega_j|^2 - |\omega_i|^2\right) = 0$, $U_{(m,n)}(t_f) \cdot U_{(i,j)}(t_f)$ is a phase gate on $\{|m\rangle, |n\rangle\}$. Thus, following the demonstration in Chapter 5.2, $U^{(D)}$ is a universal gate set on S_D.

4.2 The Zhu-Wang Scheme for Abelian Geometric Quantum Computation

An alternative approach to generating non-Abelian geometric gates is to use Abelian holonomies, but acting on a basis that is transformed from the computational basis. This was proposed in 2002 by Shi-Liang Zhu and Z. D. Wang in the context of nuclear magnetic resonance (NMR) devices [25]. In the general case, an Abelian phase gate in the $\{|\psi_0\rangle, |\psi_1\rangle\}$ basis, $e^{i\phi_0}|\psi_0\rangle\langle\psi_0| + e^{i\phi_1}|\psi_1\rangle\langle\psi_1|$, acts on the computational basis, $\{|0\rangle, |1\rangle\}$ as

$$\begin{aligned}\left(e^{i\phi_0}|\alpha|^2 + e^{i\phi_1}|\beta|^2\right)|0\rangle\langle 0| + \alpha\beta^*\left(e^{i\phi_0} - e^{i\phi_1}\right)|0\rangle\langle 1| + \\ \alpha^*\beta\left(e^{i\phi_0} - e^{i\phi_1}\right)|1\rangle\langle 0| + \left(e^{i\phi_0}|\alpha|^2 + e^{i\phi_1}|\beta|^2\right)|1\rangle\langle 1|\end{aligned} \tag{4.13}$$

under the basis transformation,

$$\begin{aligned}|\psi_0\rangle &= \alpha|0\rangle + \beta|1\rangle \\ |\psi_1\rangle &= -\beta^*|0\rangle + \alpha^*|1\rangle.\end{aligned} \tag{4.14}$$

In the case of geometric NMR gates considered by Zhu and Wang, $\alpha = \cos\left(\frac{\chi}{2}\right)$, $\beta = \sin\left(\frac{\chi}{2}\right)$, and $\phi_0 = -\phi_1 = \gamma$ where γ is the magnitude of the geometric phase, and χ can be varied by rotating the magnetic field. Note that unlike the non-Abelian holonomy explored above, the Zhu-Wang (ZW) implementation has a non-trivial dynamic phase accumulation which must be removed. In the NMR setting this is done through a series of two sequential evolutions. First, the magnetic field is set up to produce the desired gate, and the system is allowed to evolve for half of the full required time. Next, the magnetic field is negated, and the second half of the evolution is completed. The dynamic phase accumulated during the first half of the process cancels with the dynamic phase of the second half, while the geometric phases add together. The result is a purely geometric process.

The ZW scheme has an intuitive interpretation in terms of motion on the Bloch sphere. Let us orient our axes so that $|\psi_0\rangle$ is along the $+Z$ axis, $\frac{|\psi_0\rangle+|\psi_1\rangle}{\sqrt{2}}$ is along the $+X$ axis, and $\frac{|\psi_0\rangle-i|\psi_1\rangle}{\sqrt{2}}$ is along the $+Y$ axis. Then, the diagonal evolution operator $e^{-i\gamma}|\psi_0\rangle\langle\psi_0| + e^{i\gamma}|\psi_1\rangle\langle\psi_1|$ corresponds to a rotation of the state vector about the Z axis by an angle of -2γ. If this is the only gate that can be achieved by a particular setup, then the "latitude" of the state can never be changed, thus universal quantum computing is not possible. However, by changing the orientation of the magnetic field, the eigenbasis of the Hamiltonian rotates with respect to the computational basis. The result is an effective rotation of the XZ plane about the Y axis. The Z axis transforms: $Z \to Z' = Z\cos(\chi) + X\cos(\chi)$. Evolving the system under the same time evolution operator rotates the state about the new Z' axis. If $\chi = \frac{\pi}{2}$, then Z' lies along the old X axis, and the rotation will impart an effective X-rotation on the state vector. It is this freedom to orient the Z axis that makes universal quantum computing possible with Abelian holonomies.

CHAPTER 5

LINEAR OPTICAL QUANTUM COMPUTING

With qubit architectures such as trapped ions and NMR qubits having such promise, it is reasonable to ask: why try to build a quantum computer with optics? It turns out that photons has a number of distinct advantages that could be useful for quantum information systems. Along with having long decoherence times [26], photons come with the added benefit of being easily transmissible. Both of these properties make them highly desirable carriers of quantum information. However, the ability to be used for communication is relatively unique among photons, which makes them particularly useful and, in some systems, necessary.

Along with the obvious usage of transmissible qubits (so called ”flying qubits”) for long-range quantum communication, there is a more subtle application relating to scalability. Many proposals for large quantum computers involve cluster-based setups where large arrays of quantum computers operate separately, but share information via flying qubit channels. Even for non-photonic chips like trapped ion machines, such an implementation may require the ability to convert the state of the system into a different medium, such as photons, which can be sent to neighboring devices. Computers based on photonic qubits would likely not need to make such conversions.

However, with the potential benefits of photonic quantum computers comes new challenges. Part of what makes photons robust information carriers is their lack of damaging interactions with the environment. This same property makes generating multi-photon interactions very difficult. The first optical quantum computations relied on strong non-linear effects, such as cavity QED interactions [26, 27] and the Kerr effect [26], to generate photon-photon interactions that can act as a multi-qubit quantum gate. These non-linearities, however, can be difficult to achieve in practice [26].

The potential benefits of photonic quantum computing and the relative difficulty of achieving strong non-linear coupling make the call of linear optical quantum computing especially enticing. While there are numerous approaches to realize quantum computation using linear optical elements, there are two that will be considered here. The first is based on a process first proposed by Michael Reck and Anton Zeilinger [28]. This model acknowledges the universality of tunable beam splitters and phase shifters acting on an array of beams to construct circuits capable of generating arbitrary universal operations. While there are many variations of this approach, they will collectively be referred to as the Reck scheme. The second is known as the KLM protocol (appropriately named after its creators, Emanuel Knill, Raymond Laflamme and Gerard J. Milburn). The KLM protocol utilizes photodetection on ancilla photons to introduce non-linearities which enable universal computation.

5.1 Beam Splitters and Phase Shifters as Unitary Operators

A single photon can be represented as a two-level system in a number of ways. One simple way often considered when introducing concepts of quantum mechanics is the polarization. If the polarization is represented in the vertical/horizontal basis, $\{|V\rangle, |H\rangle\}$, then a diagonally polarized photon would be represented by the vector $\frac{1}{\sqrt{2}}(|V\rangle \pm |H\rangle)$. There is a mathematically equivalent way to construct a two-level system using spatial photon modes, often known as dual-rail encoding. Rather than monitoring the intrinsic polarization of the photon, we posit two possible paths, path a and path b, for the photon to take. We can denote the two paths using an orthonormal basis, $\{|a\rangle, |b\rangle\}$. If we send an input state $|in\rangle = E_{a,in}|a\rangle + E_{b,in}|b\rangle$ into a beam splitter, as pictured in Figure 5.1, the output state becomes $|out\rangle = E_{a,out}|a\rangle + E_{b,out}|b\rangle = \tau|in\rangle$, where τ is an operator representing the action of the beam splitter. Requiring that the beam splitter be lossless so that energy is conserved results in 3 relations:

$$|\tau_{a,a}|^2 + |\tau_{b,a}|^2 = 1 \qquad |\tau_{a,b}|^2 + |\tau_{b,b}|^2 = 1 \qquad \tau_{a,a}\tau_{a,b}^* + \tau_{b,a}\tau_{b,b}^* = 0 \tag{5.1}$$

Expressing the third relation in polar form ($\tau_{i,j} = |\tau_{i,j}|e^{i\phi_{i,j}}$) gives

$$|\tau_{a,a}||\tau_{a,b}|e^{i(\phi_{a,a}-\phi_{a,b})} + |\tau_{b,a}||\tau_{b,b}|e^{i(\phi_{b,a}-\phi_{b,b})} = 0. \tag{5.2}$$

This equation can be simplified to produce

$$\frac{|\tau_{a,a}|}{|\tau_{b,a}|} = \frac{|\tau_{b,b}|}{|\tau_{a,b}|}e^{i(\Phi)}, \tag{5.3}$$

where $\Phi = \phi_{b,a} + \phi_{a,b} - \phi_{a,a} - \phi_{b,b} - \pi$. Substituting in the first two relations yields two conditions:

$$\frac{1-|\tau_{b,a}|^2}{|\tau_{b,a}|^2} = \frac{1-|\tau_{a,b}|^2}{|\tau_{a,b}|^2}e^{i\Phi} \qquad \frac{|\tau_{a,a}|^2}{1-|\tau_{a,a}|^2} = \frac{|\tau_{b,b}|^2}{1-|\tau_{b,b}|^2}e^{i\Phi}, \tag{5.4}$$

the first of which requires that $|\tau_{b,a}| = |\tau_{a,b}|$, and the second ensures $|\tau_{a,a}| = |\tau_{b,b}|$. In both cases, $\Phi = 2\pi N$ for $N \in \mathbb{Z}$ is required. Imposing these conditions, the beam splitter can be reduced to the unitary operator:

$$\tau = e^{i\phi_0}\begin{pmatrix} \cos(\theta)e^{i\phi_1} & \sin(\theta)e^{i\phi_2} \\ \sin(\theta)e^{-i\phi_2} & -\cos(\theta)e^{-i\phi_1} \end{pmatrix} \tag{5.5}$$

where $\phi_0 = \frac{1}{2}(\phi_{b,a} + \phi_{a,b})$, $\phi_1 = \frac{1}{2}(\phi_{b,b} - \phi_{b,b} + \pi)$, and $\phi_2 = \frac{1}{2}(\phi_{a,b} - \phi_{b,a})$. While τ is the most general form of a beam splitter which satisfies energy conservation, it is often reduced to a unitary in terms of only two parameters, θ and ϕ, by making the assumption that the reflected beams do not acquire an additional phase. This reduced form is given by

$$\tau(\theta, \phi) = \begin{pmatrix} \cos(\theta) & \sin(\theta)e^{i\phi} \\ \sin(\theta)e^{-i\phi} & -\cos(\theta) \end{pmatrix} \tag{5.6}$$

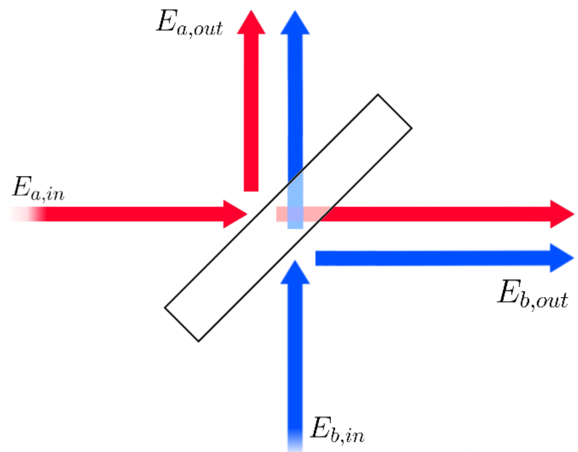

Figure 5.1 Depiction of a beam splitter acting on a dual-rail photon state.

The other optical element used in the Reck scheme is the phase shifter which, like the beam splitter, has a simple representation under dual-rail encoding. Given the two-level input $|in\rangle = E_{a,in}|a\rangle + E_{b,in}|b\rangle$, acting on $|a\rangle$ with a ϕ_a phase shifter and $|b\rangle$ with a ϕ_b phase shifter produces the output $|out\rangle = E_{a,in}e^{i\phi_a}|a\rangle + E_{b,in}e^{i\phi_b}|b\rangle$. The matrix representation of the phase shift operation, ρ, can simply be stated:

$$\rho(\phi_a, \phi_b) = \begin{pmatrix} e^{i\phi_a} & 0 \\ 0 & e^{i\phi_b} \end{pmatrix}. \tag{5.7}$$

When considering ρ as a gate, ϕ_a can be absorbed into $\phi_b = \phi$ without loss of generality.

It is worth discussing the quantum mechanical description of the dual-rail encoding. The quantum field description of light is based on the creation and annihilation of photons using creation and annihilation operators, denoted $a^\dagger$ and a respectively, and the overall state of the system is represented using the many-body Fock basis [26]. For a system in which only a single mode exists, the overall state is described by $\frac{(a^\dagger)^n}{\sqrt{n!}}|0\rangle = |n\rangle$ where $|0\rangle$ is the vacuum state and $|n\rangle$ is the state with n photon excitations. If multiple photonic modes are available, then $a_j^\dagger$ creates a photon in the j mode and $\frac{(a_j^\dagger)^n}{\sqrt{n!}}|0\rangle = |n_j\rangle$ where $|n_j\rangle$ is the state with n photons in the j mode. Likewise, $\prod_j^k \frac{(a_j^\dagger)^{n_j}}{\sqrt{n_j!}}|0\rangle = |(n_1)_1 (n_2)_2 \ldots (n_k)_k\rangle$ denotes the state with n_j photons in the j mode. The general operation of the creation and annihilation operators acting on a state is

$$a_j^\dagger |n_j\rangle = \sqrt{n_j+1}\,|(n+1)_j\rangle \qquad\qquad a_j |n_j\rangle = \sqrt{(n_j)}\,|(n-1)_j\rangle\,. \tag{5.8}$$

An arbitrary unitary operator, U, acting on the state $|(n_1)_1\,(n_2)_2\ldots(n_k)_k\rangle$ has an output given by

$$\prod_j^k \frac{\left(\sum_i U_{i,j}a_i^\dagger\right)^{n_j}}{\sqrt{n_j!}}\,|0\rangle\,. \tag{5.9}$$

We can now apply the quantum field formulation for photons to the dual-rail encoding. Specifically, we denote a photon in path 0 with $a_0^\dagger|0\rangle = |1_0\rangle$ and path 1 with $a_1^\dagger|0\rangle = |1_1\rangle$ so that the general quantum dual-rail state is given by

$$\frac{\left(a_0^\dagger\right)^m}{\sqrt{m!}}\frac{\left(a_1^\dagger\right)^n}{\sqrt{n!}}\,|0\rangle = |m_0 n_1\rangle\,. \tag{5.10}$$

The result of a beam splitter acting on the input state, Eq. (5.10) can be represented, using Eq. (5.9), as

$$\frac{\left(\cos(\theta)a_0^\dagger + \sin(\theta)e^{i\phi}a_1^\dagger\right)^m}{\sqrt{m!}}\frac{\left(\sin(\theta)e^{-i\phi}a_0^\dagger - \cos(\theta)a_1^\dagger\right)^n}{\sqrt{n!}}\,|0\rangle\,. \tag{5.11}$$

Similarly the output of a phase shifter is given by

$$\frac{\left(a_0^\dagger\right)^m}{\sqrt{m!}}\frac{\left(e^{i\phi}a_1^\dagger\right)^n}{\sqrt{n!}}\,|0\rangle\,. \tag{5.12}$$

5.2 The Reck Scheme

While it has long been known that any energy conserving process can be represented with a unitary operator, the inverse was not confirmed until the end of the 20$^{\text{th}}$ century. In 1994, Michael Reck, Anton Zeilinger, Herbert Bernstein, and Philip Bertani demonstrated that the successive application of lossless two-dimensional beam splitters and phase shifters could realize any $N \times N$ unitary operator [28]. They proposed an algorithm, referred to here as the Reck Scheme, which factors a given unitary into a sequence of dual-rail beam splitters. The algorithm is most easily considered in the framework of classical optics, so this is where we will focus.

First, it is necessary to upgrade the dual-rail system to an N rail system. The N possible paths of the system are represented by the states $\{|n\rangle \mid n \in \mathbb{Z} \;\&\; n \in [0, N-1]\}$. Define the operator, $T_{i,j}(\theta,\phi)$ as

$$T_{i,j} = \left(\sum_{k,m \in i,j} \left(\rho(\phi,0)\tau(\theta,0)\right)_{k,m} |k\rangle \langle m| \right) + \sum_{k \notin i,j} |k\rangle \langle k| \,. \tag{5.13}$$

This corresponds to the application of a beam splitter between path i and path j, followed by a phase shifter on path i. The matrix representation of $T_{i,j}(\theta, \phi)$ on the $\{i, j\}$ subspace of the N-rail system is:

$$\rho(\phi,0)\tau(\theta,0) = \begin{pmatrix} e^{i\phi}\cos(\theta) & e^{i\phi}\cos(\theta) \\ \sin(\theta) & -\cos(\theta) \end{pmatrix}, \tag{5.14}$$

while the rest of the system sees the identity operator. The algorithm devised by Reck uses sequential applications of $T_{i,j}(\theta, \phi)$, followed by a phase shift gate on each rail, to generate the desired unitary operator, U.

The first step is to multiply $\prod_{j=1}^{N-1} T_{N,N-j}(\theta_{N,N-j}, \phi_{N,N-j})$ on the right of U giving a new unitary operator, U'. Note that here the objects are one-indexed so that the first row of U is $U_{1,j}$ and the last row is $U_{N,j}$. By precisely tuning the T's, this operation can set all of the non-diagonal elements in the last row and last column to zero. The $U'_{N,N}$ element then takes a value given by $e^{i\gamma_N}$. Moreover, the first $N-1$ rows and columns of U' become a new $N-1$ dimensional unitary operator. The process is then repeated for this $N-1$ dimensional unitary. Specifically, $\prod_{j=2}^{N-1} T_{N-1,N-j}(\theta_{N-1,N-j}, \phi_{N-1,N-j})$ is applied to U'. As before, this reduces the $N-1$ row and $N-1$ column to a single non-zero element on the diagonal given by $e^{i\gamma_{N-1}}$. This is repeated until the resulting operator is fully diagonalized. At this point, the application of a phase shifter, P, on each rail independently produces the identity so long as $P_{j,k} = e^{-i\gamma_j}\delta_{j,k}$. The whole algorithm can be represented mathematically as

$$U\left(T_{N,N-1}T_{N,N-2}\dots T_{N,1}T_{N-1,N-2}\dots T_{2,1}P\right) = I. \tag{5.15}$$

Thus, $U^\dagger$ has been produced. U can then be acquired through conjugation:

$$\begin{aligned} U &= \left(T_{N,N-1}T_{N,N-2}\dots T_{N,1}T_{N-1,N-2}\dots T_{2,1}P\right)^\dagger \qquad (5.16)\\ &= P^\dagger \left(T^\dagger_{2,1}T^\dagger_{3,1}T^\dagger_{3,2}\dots T^\dagger_{N,N-2}T^\dagger_{N,N-1}\right). \qquad (5.17) \end{aligned}$$

To see why this process works, note that

$$U'_{N,i} \equiv \left(U \prod_{j=1}^{N-1} T_{N,N-j}(\theta_{N,N-j}, \phi_{N,N-j}) \right)_{N,i} = \langle U_N | V_i \rangle \tag{5.18}$$

where $\{|V_i\rangle \mid i \in \mathbb{Z} \;\&\; i \in [1,N]\}$ is a tunable set of orthonormal vectors and U_N is the N^{th} row of U. Through careful selection of $\theta_{N,N-j}$ and $\phi_{N,N-j}$, $|V_N\rangle$ can be chosen so that $|\langle U_N | V_N \rangle| = 1$. Because

$\langle V_i|V_j\rangle = \delta_{i,j}$, this choice guarantees that $|\langle U_N|V_j\rangle| = \delta_{N,j}$. Thus, the only non-zero element of U'_N is $U'_{N,N}$, the element on the diagonal. Moreover, the same outcome will occur on the N^{th} column of U' because it is unitary.

One thing to note about this encoding is that each path for the photon corresponds to a single element of the overall state vector. Thus, the number of paths required to store the information of a D qubit system grows as 2^D. Similarly, the number of beam splitters (and phase shifters) grows exponentially as well. Of course, when using this method to design classical circuits, the universality of light becomes extremely powerful. Designing and building nanophotonic devices which implement this style of computation is an active area of research [29].

5.3 The KLM Protocol

Unlike the Reck scheme which has merit in both the classical and quantum regime of optics, the KLM protocol functions only in the quantum regime, and its primary use is quantum information processing. The immediate benefit of this is that the resource cost scales linearly with qubit number rather than exponentially. The KLM protocol uses a dual-rail encoding to store the information of a qubit. Specifically, the logical $|0\rangle$ state is defined as the dual-rail Fock state $|1_0 0_1\rangle = a_0^\dagger |0_v\rangle$, and the logical $|1\rangle$ state is defined as $|0_0 1_1\rangle = a_1^\dagger |0_v\rangle$. Note that here, $|0_v\rangle$ is used to denote the many-body vacuum state to avoid confusion with the logical $|0\rangle$ state.

Beam splitters and phase shifters acting between the two rails of a qubit are sufficient to realize universal single qubit logic. While this may be intuitive in light of the Reck scheme, proving it for this particular context may be insightful. Recall the output of a beam splitter acting on the dual-rail Fock state given in Eq. (5.11). For the KLM protocol, the single qubit input state is guaranteed to have $m + n = 1$. For the $m = 1, n = 0$ case, the logical input is $|0\rangle$ and the output is $\cos(\theta)a_0^\dagger |0_v\rangle + e^{i\phi}\sin(\theta)a_1^\dagger |0_v\rangle = \cos(\theta)|0\rangle + e^{i\phi}\sin(\theta)|1\rangle$. Similarly, for $m = 0, n = 1$, the logical input is $|1\rangle$ and the output is $e^{-i\phi}\sin(\theta)a_0^\dagger |0_v\rangle - \cos(\theta)a_1^\dagger |0_v\rangle = e^{-i\phi}\sin(\theta)|0\rangle - \cos(\theta)a_1^\dagger |1\rangle$. It follows that the quantum beam splitter acts on the qubit according to the matrix in Eq. (5.6). Note that while in the case that $m + n = 1$ the many-body operator is equivalent to the classical operator, this is not true in general. With the action of the beam splitter established, it is simple enough to show that a 50/50 beam splitter with $\theta = \frac{\pi}{4}$ and $\phi = 0$ gives a Hadamard gate. Next, we consider the operation associated with a phase shifter on the qubit. Using the same approach as the beam splitter, it is straightforward to show using Eq. (5.12) that the phase shifter acts on the qubit according to the matrix in Eq. (5.7). Therefore, the phase shifter can be used (as may have been expected) to implement a Phase gate. With these two gates available to the system, it is clear that we can perform universal single qubit logic on the quantum dual-rail qubit.

The main challenge, as with other attempts to use photons as qubits, is to achieve an interaction capable of mixing the logic states. In the KLM protocol, this mixing operator will be in the form of a CZ gate. What makes this possible is a non-linear single qubit operator known as the non-linear sign-shift gate (NS), which converts the state $\alpha\left|0_v\right\rangle + \beta\left(a^\dagger\right)\left|0_v\right\rangle + \gamma\left(a^\dagger\right)^2\left|0_v\right\rangle$ to the state $\alpha\left|0_v\right\rangle + \beta\left(a^\dagger\right)\left|0_v\right\rangle - \gamma\left(a^\dagger\right)^2\left|0_v\right\rangle$ [26]. Equipped with this gate, we can begin constructing a CZ gate. The system starts in the two qubit state $\alpha\left|1_0 0_1\right\rangle_0\left|1_0 0_1\right\rangle_1 + \beta\left|1_0 0_1\right\rangle_0\left|0_0 1_1\right\rangle_1 + \gamma\left|0_0 1_1\right\rangle_0\left|1_0 0_1\right\rangle + \delta\left|0_0 1_1\right\rangle_0\left|0_0 1_1\right\rangle_1$, illustrated in Figure 5.2. It will be useful to express this in terms of the creation and annihilation operators:

$$\left(\alpha\left(a^\dagger_{0,0}\right)\left(a^\dagger_{0,1}\right) + \beta\left(a^\dagger_{0,0}\right)\left(a^\dagger_{1,1}\right) + \gamma\left(a^\dagger_{1,0}\right)\left(a^\dagger_{0,1}\right) + \delta\left(a^\dagger_{1,0}\right)\left(a^\dagger_{1,1}\right)\right)\left|0_v\right\rangle \tag{5.19}$$

where $a^\dagger_{i,j}$ creates a photon in the i rail of the j photon.

Figure 5.2 Shows the dual-rail system for two KLM qubits.

The first step of the operation is to insert a beam splitter with $\phi = 0$ and $\theta = \frac{\pi}{4}$ between the 1 rail of the 0 qubit and the 1 rail of the 1 qubit. This connection is shown in Figure Figure 5.3 for clarity. As a result, the creation operators undergo a transformation:

$$\begin{aligned} a^\dagger_{0,0} &\to a^\dagger_{0,0} & a^\dagger_{0,1} &\to a^\dagger_{1,0} \\ a^\dagger_{1,0} &\to \frac{1}{\sqrt{2}}\left(a^\dagger_{1,0} + a^\dagger_{1,1}\right) & a^\dagger_{1,1} &\to \frac{1}{\sqrt{2}}\left(a^\dagger_{1,0} - a^\dagger_{1,1}\right). \end{aligned} \tag{5.20}$$

Following this transformation, the state of the system becomes

$$\begin{aligned} &\left(\alpha\left(a^\dagger_{0,0}\right)\left(a^\dagger_{0,1}\right) + \frac{1}{\sqrt{2}}\beta\left(a^\dagger_{0,0}\right)\left(a^\dagger_{1,0}\right) - \frac{1}{\sqrt{2}}\beta\left(a^\dagger_{0,0}\right)\left(a^\dagger_{1,1}\right) + \right. \\ &\left.\frac{1}{\sqrt{2}}\gamma\left(a^\dagger_{1,0}\right)\left(a^\dagger_{0,1}\right) + \frac{1}{\sqrt{2}}\gamma\left(a^\dagger_{0,1}\right)\left(a^\dagger_{1,1}\right) + \frac{1}{2}\delta\left(a^\dagger_{1,0}\right)^2 - \frac{1}{2}\delta\left(a^\dagger_{1,1}\right)^2\right)\left|0_v\right\rangle. \end{aligned} \tag{5.21}$$

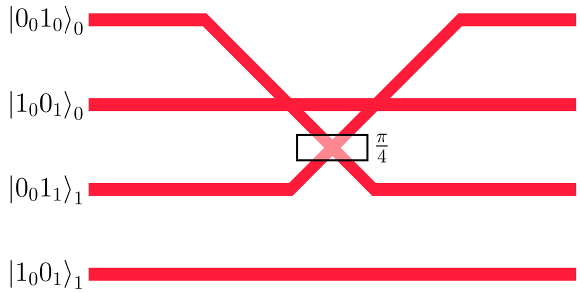

Figure 5.3 First step to implement a CZ gate for two KLM qubits. A $\theta = \frac{\pi}{4}$ beam splitter is between the 1 rail of the 0 qubit and the 1 rail of the 1 qubit.

It is interesting to note that at this point in the circuit, the qubits are no longer normalized. In fact, we now see where the NS gate is able to have an effect. Specifically, there are two terms with $\left(a^\dagger\right)^2$, which will be negated with the application of an NS gate. Perhaps to be expected, this is the next step in the application of a CZ gate: the 1 rail of the 0 qubit and the 1 rail of the 1 qubit are both acted on by an NS gate. The full circuit up to this point is illustrated in Figure 5.4. This step transforms the squared creation operators according to

$$\left(a^\dagger_{1,0}\right) \to -\left(a^\dagger_{1,0}\right) \qquad\qquad \left(a^\dagger_{1,1}\right) \to -\left(a^\dagger_{1,1}\right), \tag{5.22}$$

and all other terms are left unchanged. Of course, if there were more squared terms, those would be negated as well. The state of the system following this step is now

$$\begin{aligned}&\left(\alpha\left(a^\dagger_{0,0}\right)\left(a^\dagger_{0,1}\right) + \frac{1}{\sqrt{2}}\beta\left(a^\dagger_{0,0}\right)\left(a^\dagger_{1,0}\right) - \frac{1}{\sqrt{2}}\beta\left(a^\dagger_{0,0}\right)\left(a^\dagger_{1,1}\right) + \right.\\ &\left.\frac{1}{\sqrt{2}}\gamma\left(a^\dagger_{1,0}\right)\left(a^\dagger_{0,1}\right) + \frac{1}{\sqrt{2}}\gamma\left(a^\dagger_{0,1}\right)\left(a^\dagger_{1,1}\right) - \frac{1}{2}\delta\left(a^\dagger_{1,0}\right)^2 + \frac{1}{2}\delta\left(a^\dagger_{1,1}\right)^2\right)|0_v\rangle\,.\end{aligned} \tag{5.23}$$

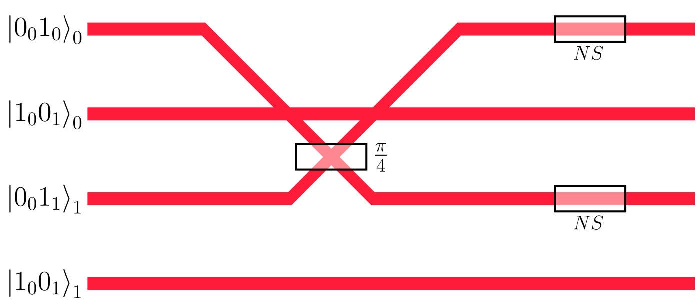

Figure 5.4 The second step required to implementing a CZ gate for two KLM qubits. An NS gate is inserted on the 1 rail of the 0 qubit and the 1 rail of the 1 qubit.

There is only one more step, which is to insert a second beam splitter, also with $\phi = 0$ and $\theta = \frac{\pi}{4}$, between the 1 rail of the 0 qubit and the 1 rail of the 1 qubit. This step is shown along with the full circuit in Figure 5.5. Following from the first step, this beam splitter transforms the creation operators according to Eq. (5.20). The state simplifies nicely after this transformation, yielding:

$$\left(\alpha \left(a^\dagger_{0,0}\right)\left(a^\dagger_{0,1}\right) + \beta \left(a^\dagger_{0,0}\right)\left(a^\dagger_{1,1}\right) + \gamma \left(a^\dagger_{1,0}\right)\left(a^\dagger_{0,1}\right) - \delta \left(a^\dagger_{1,0}\right)\left(a^\dagger_{1,1}\right)\right)|0_v\rangle\,. \tag{5.24}$$

In the $\{|0\rangle, |1\rangle\}$ representation, we have converted the input state,
$\alpha |0\rangle_0 |0\rangle_1 + \beta |0\rangle_0 |1\rangle_1 \gamma |1\rangle_0 |0\rangle_1 + \delta |1\rangle_0 |1\rangle_1$, to the output state,
$\alpha |0\rangle_0 |0\rangle_1 + \beta |0\rangle_0 |1\rangle_1 \gamma |1\rangle_0 |0\rangle_1 - \delta |1\rangle_0 |1\rangle_1$. Thus, we have performed a CZ gate on the input state.

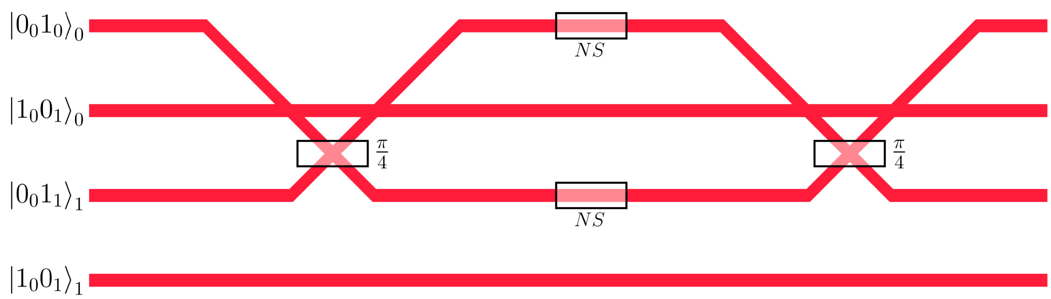

Figure 5.5 The final step to implement a CZ gate for two KLM qubits. A $\theta = \frac{\pi}{4}$ beam splitter is between the 1 rail of the 0 qubit and the 1 rail of the 1 qubit.

The only element not yet detailed is the NS gate. As discussed above, the role of the NS gate is to transform an input state, $|in\rangle \equiv \left(\alpha + \beta\left(a^\dagger_{in}\right) + \gamma\left(a^\dagger_{in}\right)^2\right)|0_v\rangle$, to the corresponding output state, $|in\rangle \equiv \left(\alpha + \beta\left(a^\dagger_{in}\right) - \gamma\left(a^\dagger_{in}\right)^2\right)|0_v\rangle$ where $a^\dagger_{in}$ creates a photon on the input rail. The circuit requires the use of two ancilla rails, c_0 and c_1. c_0 is innitialized with a single photon and c_1 is initialized with zero photons. The total many-body Fock state corresponding to the initial configuration of the three rail system is given:

$$\left(\alpha\left(a^\dagger_{c_0}\right) + \beta\left(a^\dagger_{c_0}\right)\left(a^\dagger_{in}\right) + \gamma\left(a^\dagger_{c_0}\right)\left(a^\dagger_{in}\right)^2\right)|0_v\rangle \tag{5.25}$$

An application of the NS gate requires a total of three beam splitters. The first is applied to the two ancilla rails, followed by a second beam splitter between the input rail and the c_0 ancilla rail, and a final beam splitter applied between the two ancilla rails. After these three beam splitters, the three rail state consists of a superposition of 19 possible states. However, the number of possible output states can be reduced by inserting photodetectors on the output of the ancilla rails. For a visual representation of the NS circuit, see Figure 5.6. By only accepting outputs in which exactly one photon was detected on c_0 and zero photons were detected on c_1, the output is reduced to only three superposed states:

$$\left(\alpha\omega_0\left(a^\dagger_{c_0}\right) + \beta\omega_1\left(a^\dagger_{c_0}\right)\left(a^\dagger_{in}\right) + \gamma\omega_2\left(a^\dagger_{c_0}\right)\left(a^\dagger_{in}\right)^2\right)|0_v\rangle \tag{5.26}$$

where

$$\omega_0 = \sin(\theta_1)\sin(\theta_3) - \cos(\theta_1)\cos(\theta_2)\cos(\theta_3), \quad \omega_1 = \sin(\theta_1)\cos(\theta_2)\sin(\theta_3) - \cos(\theta_1)\cos(2\theta_2)\cos(\theta_3),$$
$$\omega_2 = \frac{1}{2}\cos(\theta_2)\left(\cos(\theta_1)(1-3\cos(2\theta_2))\cos(\theta_3) + 2\sin(\theta_1)\cos(\theta_2)\sin(\theta_3)\right). \tag{5.27}$$

Here, θ_i corresponds to the i^{th} beam splitter in the sequence. The problem of realizing an NS gate now reduces to the problem of forcing $\omega_0 = \omega_1 = -\omega_2$ with $|\omega_i|^2 = p$, the probability of measuring $|1_{c_0}0_{c_1}\rangle$. This system of equations can be solved to give $\theta_1 = \theta_3 = \frac{3\pi}{8}$, $\theta_2 = \arccos(1+\sqrt{2})$, and $p = \frac{1}{4}$. Thus, with correctly tuned beam splitters, the NS gate can be performed with a success rate of $\frac{1}{4}$, and the CZ gate with a success rate of $\frac{1}{16}$. Critically, successful operations are heralded by measurement outcomes of the ancilla states so that unsuccessful attempts can be ignored.

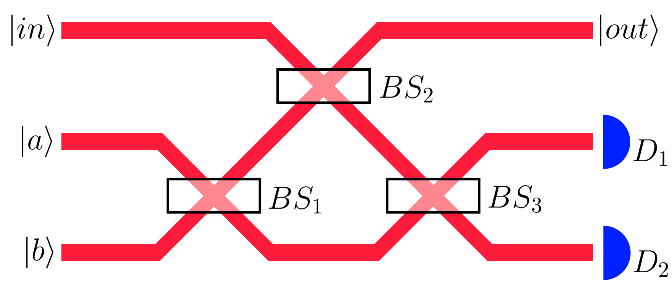

Figure 5.6 The Non-Linear Sign Shift Gate $|in\rangle$ is the input state, and $|a\rangle$ and $|b\rangle$ are ancilla states with $|a\rangle = |1\rangle$ and $|b\rangle = |0\rangle$. The detectors, D_1 and D_2 are destructive measurement devices which introduce non-linearity.

CHAPTER 6

GEOMETRIC OPTICAL PHASE AND HOLONOMIC QUANTUM COMPUTING WITH LIGHT

Having established the traditional techniques used to do quantum computing with optics, we now turn to introduce holonomic quantum computing in an optical setting. First, however, it is necessary to consider how the quantum phenomena required for holonomic quantum computation can manifest in optical systems. Some of the first examples of quantum phenomena involved the demonstration of "optical effects" using particles such as electrons. The Young double-slit experiment, for example, was a key experiment demonstrating the wave nature of light. Nearly 100 years later, electrons were shown to exhibit the same wave-like behavior. While these properties are often taken for granted, there are many analogues between classical optics and quantum mechanics that can be exploited today.

6.1 Geometric Phase of an Evolving Plane Wave

As mentioned in Chapter 3, the geometric phase of a two level quantum system is equal to the solid angle traversed by the state during its evolution. It turns out that this holds true for a photon polarization traversing the Poincaré sphere as well. One easy medium to examine this property is the propagation of a plane wave through an anisotropic material. Specifically, the polarization of the wave can be tracked on the Poincaré sphere as the beam evolves, and the geometric phase can be calculated and compared to the solid angle enclosed by the path. We demonstrate this through the consideration of a polarized beam propagating through a slab of material with gyrotropic permittivity. This property is a type of circular birefringence, where the refractive index varies between the left and right circularly polarized components of a wave. The constitutive relations for such a material are given by

$$\vec{D} = \epsilon_0 \vec{E} - \epsilon_0 g i \left(\vec{e}_z \times \vec{E} \right), \qquad \vec{B} = \mu_0 \vec{E} - \mu_0 g i \left(\vec{e}_z \times \vec{H} \right), \tag{6.1}$$

where g is a measure of the strength of the birefringence. Taking solutions of the form, $\vec{E} = E(x, y, \vec{z}) e^{-i\omega t}$, the Maxwell's equations become

$$\nabla \times \vec{E} = i\omega\mu_0 \left(\vec{H} - gi\vec{e}_z \times \vec{H} \right) \tag{6.2}$$

$$\nabla \times \vec{H} = -i\omega\epsilon_0 \left(\vec{E} - gi\vec{e}_z \times \vec{E} \right) \tag{6.3}$$

$$\nabla \cdot \vec{E} = \nabla \cdot \left(gi\vec{e}_z \times \vec{E} \right) \tag{6.4}$$

$$\nabla \cdot \vec{H} = \nabla \cdot \left(gi\vec{e}_z \times \vec{H} \right). \tag{6.5}$$

Combining Eq. (6.2) and Eq. (6.3), and assuming $E_z = H_z = 0$, gives the equation of motion for the transverse electric field within the gyrotropic material:

$$\partial_{z,z}\vec{E}_\perp = -k^2(1+g^2)\vec{E}_\perp + 2k^2 g\boldsymbol{\sigma}_2\vec{E}_\perp \tag{6.6}$$

Where $\boldsymbol{\sigma}_2 \equiv \begin{pmatrix} 0 & -i \\ i & 0 \end{pmatrix}$ is the second Pauli matrix and $k = \frac{\omega}{c}$. If $\vec{E}(x,y,z)$ is then restricted to plane-waves of the form $\vec{E}(x,y,z) = \vec{n}E_0 e^{ik_g z}$, the equation of motion can be reduced to the eigenvalue problem,

$$k_g^2\vec{n} = \boldsymbol{V}\vec{n}. \tag{6.7}$$

Here, $\boldsymbol{V} = k^2\left(1+g^2\right)\boldsymbol{\sigma}_0 - 2g\boldsymbol{\sigma}_2$ and $\vec{n}$ is the polarization of the plane wave. This system has eigenvectors $\vec{R}$ and $\vec{L}$ with eigenvalues $k^2(g-1)^2$ and $k^2(g+1)^2$ respectively. Here, $\vec{R}$ and $\vec{L}$ are the right and left circular polarization vectors (the eigenvectors of $\boldsymbol{\sigma}_2$). Given an initial condition that is a linear combination of these basis vectors, $\vec{E_i} \equiv \alpha\vec{R} + \beta\vec{L}$, it will propagate in z as

$$\vec{E} = e^{ik_{g,R}z}\alpha\vec{R} + e^{ik_{g,L}z}\beta\vec{L} \tag{6.8}$$

$$\vec{E} = e^{ik(1-g)z}\alpha\vec{R} + e^{ik(1+g)z}\beta\vec{L} \tag{6.9}$$

where Eq. (6.9) assumes that $g \leq 1$. On the polarization Poincaré sphere, this evolution corresponds to rotations about the y-axis, given (up to the overall phase factor, e^{ikz}) by $e^{-ikgz\boldsymbol{\sigma}_z}$. The magnitude of the geometric phase is then half of the surface area enclosed by the path of the evolving spin on the Poincaré sphere. To verify this, it is first necessary to determine this surface area. The simplest case to consider is $kgz = \pi$, where the polarization returns to its initial configuration. In this case, the surface area is given by $\Omega \equiv 4\pi\sin^2\left(\frac{\alpha}{2}\right)$, where α is the angle between the polarization state and the y-axis. For an initial polarization $\vec{s_i} \equiv \cos(\theta)\vec{H} + e^{i\phi}\sin(\theta)\vec{V}$, α is given by

$$\alpha = \arccos\left(-2\cos(\theta)\sin(\theta)\sin(\phi)\right). \tag{6.10}$$

Thus, the accumulated geometric phase can be determined:

$$\Phi_g = \frac{\Omega}{2} = 2\pi\sin^2\left(\frac{1}{2}\alpha\right). \tag{6.11}$$

In order to test this, numerically computed data calculated using Eq. (3.22) was compared to the result of Eq. (6.11). Figure 6.1(a) shows both of these values for the geometric phase accumulated by a plane wave after traversing a gyrotropic slab for a full cycle in polarization space.

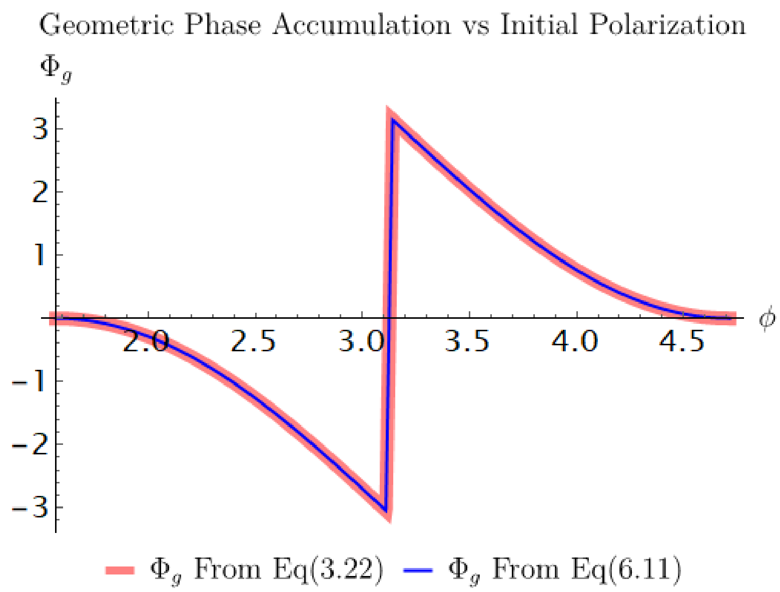

(a)

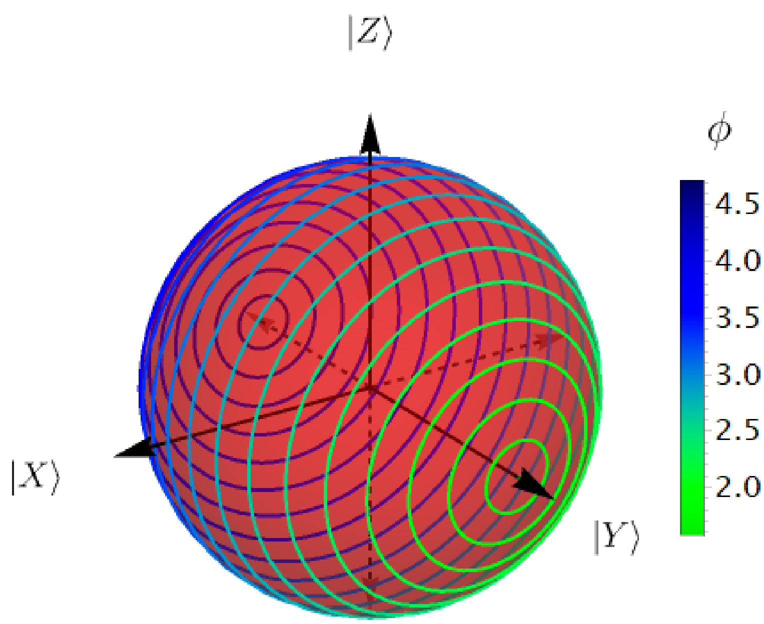

(b)

Figure 6.1 (a) Shows geometric phase calculated using Eq. (6.11) compared to numerical data computed using Eq. (3.22). The initial polarization angle, θ, is held fixed while the initial ellipticity, ϕ, is varied from $\frac{\pi}{2}$ to $\frac{3\pi}{2}$. (b) Shows the path taken in polarization space given the initial ellipticity ϕ.

6.2 The Paraxial Equation

Another key analog to quantum physics found in optics arises from the paraxial equation. For beams propagating in a particular manner, the Maxwell equations can be approximated by an effective Schrödinger equation acting in two spatial dimensions. Not only is this powerful in that it allows us to treat a spatial variance on a laser beam as a quantum mechanical system, but it also provides an environment in which two-dimensional quantum physics can be analyzed and physically explored. The paraxial equation arises from Maxwell's equations for free space after applying the paraxial approximation:

$$\partial_{z,z}\psi << k\partial_z\psi. \tag{6.12}$$

In the Lorentz gauge, the Maxwell equations can be expressed as

$$\nabla^2 A - \frac{1}{c^2}\partial_{t,t}A = 0, \qquad \nabla^2\Phi - \frac{1}{c^2}\partial_{t,t}\Phi = 0. \tag{6.13}$$

Focus on the left equation in Eq. (6.13), and let $A = R(r)T(t)$. Then the wave equation becomes

$$\frac{\nabla^2 R}{R} = \frac{1}{c^2 T}\partial_{t,t}T = -k^2, \tag{6.14}$$

leaving the Helmholtz equation for the spatial field:

$$(\nabla^2 + k^2)R = 0 \tag{6.15}$$

If R is assumed to take the form,

$$R = \psi(r,z)e^{ikz}, \tag{6.16}$$

then the Helmholtz equation becomes:

$$\nabla^2\psi + 2ik\partial_z\psi = 0. \tag{6.17}$$

Finally, enforcing the paraxial approximation of Eq. (6.12) gives the paraxial equation:

$$\nabla_\perp^2\psi + 2ik\partial_z\psi = 0, \tag{6.18}$$

where $\nabla_\perp^2 \equiv \partial_{x,x} + \partial_{y,y}$.

Eq. (6.18) shows the analytical power of the paraxial approximation: the spatial wave equation has reduced to the Schrödinger equation for a free particle in 2D space [30], revealing a connection between the behavior of quantum mechanical particles and classical propagating waves.

6.3 Solutions to the Paraxial Equation

We can now begin uncovering the form of $\psi(r, z)$, the solution to the paraxial equation. Begin by expressing $\psi(r, z)$ in terms of $\tilde{\psi}(p, z)$, its spatial Fourier transform:

$$\psi(r, z) = \frac{1}{2\pi} \int\int \tilde{\psi}(p, z) e^{ip \cdot \frac{r}{w_o}} d^2p, \tag{6.19}$$

where w_0 is the beam waist. Applying the same transformation to the paraxial equation, it is clear that $\tilde{\psi}(p, z)$ satisfies

$$\left(-\frac{p^2}{w_0^2} + 2ik\partial_z \right) \tilde{\psi}(p, z) = 0. \tag{6.20}$$

Taking the ansatz $\tilde{\psi}(p, z) = \phi(p) e^{\frac{i\alpha z}{k w_0^2}}$, Eq. (6.20) gives

$$p^2 + 2\alpha = 0 \tag{6.21}$$

$$\implies \alpha = -\frac{1}{2} p^2. \tag{6.22}$$

This form satisfies the spatially Fourier transformed paraxial equation. We can construct an integral equation by inserting this ansatz into Eq. (6.19) and noting that

$$\phi(p) = \tilde{\psi}(p, 0) = \frac{1}{2\pi} \int\int \psi(r, 0) e^{-ip \cdot \frac{r}{w_0}} d^2r. \tag{6.23}$$

With this, Eq. (6.19) becomes

$$\psi(r, z) = \frac{1}{(2\pi)^2} \int\int \left(\int\int \psi(r', 0) e^{-i \frac{p^2}{2k w_0^2} z} e^{-ip \cdot \frac{r'}{w_0}} d^2r' \right) e^{ip \cdot \frac{r}{w_o}} d^2p. \tag{6.24}$$

After rearranging, this equation takes the intuitive form:

$$\psi(r, z) = \int\int \psi(r', 0) G(r - r', z) d^2r' \tag{6.25}$$

where

$$G(r, z) = \frac{1}{(2\pi)^2} \int\int e^{-i \frac{p^2}{2k w_0^2} z} e^{ip \cdot \frac{r}{w_0}} d^2p. \tag{6.26}$$

The integral in Eq. (6.26) can be evaluated, giving

$$G(r,z) = -\frac{iw_0^2}{\lambda z} e^{i\frac{\pi}{\lambda z} r^2}, \tag{6.27}$$

with $\lambda = \frac{2\pi}{k}$. From the form of Eq. (6.25), it is clear that $G(r,z)$ is the paraxial Green function, and the particular solution $\psi(r,z)$ is obtained through convolution with an initial condition, $\psi(r,0)$. If the $\psi(r,0)$ is taken to have a Gaussian structure,

$$\psi(r,0) = e^{-\left(\frac{r}{w_0}\right)^2}, \tag{6.28}$$

then the output will have the form of a Gaussian beam. If, instead, $\psi(r,0)$ is a Gaussian times another spatially varying function, then arbitrary Gaussian modes can be produced. For example, consider $\psi(r,0) = u(r)_p^l e^{-r^2}$ where

$$u(r)_p^l = \frac{2^{\frac{1}{2}(3+|l|)}}{w_0^{2+|l|}} \sqrt{\pi}\,(x+iy)^l \sqrt{\frac{p!}{(|l|+p)!}} L_p^{|l|}\left(\frac{2r^2}{w_0^2}\right), \tag{6.29}$$

with $L_p^{|l|}(x)$, the Laguerre polynomial. This initial condition produces the general Laguerre-Gaussian (LG) beam with radial index p and azimuthal index l, given by

$$C_p^{|l|} \frac{w_0}{w(z)} \left(\frac{r\sqrt{2}}{w(z)}\right)^{|l|} e^{-r^2\left(\frac{1}{w(z)^2} + \frac{ik}{2R(z)}\right)} e^{i(\gamma(z) - l\phi)} L_p^{|l|}\left(\frac{2r^2}{w(z)^2}\right), \tag{6.30}$$

where $w(z)$ is the beam radius ($w(0) \equiv w_0$), $R(z)$ is the radius of curvature, $\gamma(z)$ is the Gouy phase, ϕ is the polar angle, and $C_p^{|l|}$ is a normalization coefficient.

6.4 Harmonic Dielectric Trap

The free space paraxial equation provides a useful analogue to the two-dimensional free space Schrödinger equation. It is thus natural to consider systems in which wave propagation can be compared to a quantum particle under the influence of a nonzero potential. An interesting case to consider is the simple harmonic oscillator, a canonical problem in physics. A quantum particle under the influence of a harmonic potential in 2D space evolves under the Hamiltonian given by

$$H = -\frac{1}{2m}\nabla_\perp^2 + \frac{1}{2}k_f r^2, \tag{6.31}$$

resulting in the time-dependant, two-dimensional Schrödinger equation,

$$\left(-\frac{1}{2m}\nabla_\perp^2 + \frac{1}{2}k_f r^2\right)|\psi(t)\rangle = i\hbar\partial_t|\psi(t)\rangle, \tag{6.32}$$

where k_f is the force constant related to the potential.

To replicate this form in the optics setting, the paraxial equation must be extended to include a term for a constant potential. This can be achieved by considering propagation through a material, rather than propagation in free space. In particular, take a spatially inhomogeneous medium with refractive index of the form:

$$n(r)^2 = n_0^2(1 - \Omega^2 r^2). \tag{6.33}$$

Provided that $\Omega << k$ (k is the free-space wave number), this refractive index corresponds to a paraxial equation given by

$$-\frac{1}{2kn_0}\nabla_\perp^2\psi + \frac{n_0}{2}k\Omega^2 r^2\psi = i\partial_z\psi, \tag{6.34}$$

where n_0 is the index of refraction at $r = 0$ and Ω relates to the material's focusing properties [31]. Comparing this to Eq. (6.32), it is clear that a beam propagating through such a material behaves as a particle in a quantum Harmonic trap with $m = \frac{1}{kn_0}$, $k_f = n_0\Omega^2 k$, and $\hbar = 1$. The Hamiltonian governing this system is independent of time, therefore the stationary states can be determined using the time-dependent Schrödinger equation. With this approach, it can be shown using direct substitution that the LG function beam is a stationary state of the trapped paraxial equation, with eigenvalues given by [31]

$$\epsilon_{l,p} = \frac{\Omega}{k}(|l| + 2p + 1) \tag{6.35}$$

Note that turning to the time-dependent Schrödinger equation to identify stationary states is equivalent to restricting the time-independent Schrödinger equation to solutions of the form: $\psi(r,z) = \phi(r)e^{-(i\epsilon_{l,p}z)}$.

An important realization is that the LG modes form an orthonormal basis spanning a countably infinity Hilbert space, S. With this in mind, it is natural to construct a finite n dimensional subspace of S, call it s_{beam}, containing the set of LG modes postulated to be available for a given system:
$s_{beam} \equiv \{|\psi_{l_i,p_i}\rangle \mid i \in \mathbb{Z} \text{ and } i \in [0, k-1]\}$. Of course, $|\psi_{l_i,p_i}\rangle$ represents the LG mode with $l = l_i$ and $p = p_i$. With this in mind, we can represent the dielectric harmonic trap Hamiltonian corresponding to the time-dependent Schrödinger equation as an operator acting on s_{beam}:

$$H \equiv \sum_i \epsilon_{l_i,p_i} |\psi_{l_i,p_i}\rangle \langle\psi_{l_i,p_i}| \,. \tag{6.36}$$

6.5 Holonomic Gates on Trapped LG Modes

Consider the time evolution associated with the Hamiltonian for the harmonic dielectric trap:

$$U(z) = \sum_j e^{iz\epsilon_{l_j,p_j}} |\psi_{l_j,p_j}\rangle \langle\psi_{l_j,p_j}| = \sum_j e^{i\zeta(|l_j|+2p_j+1)} |\psi_{l_j,p_j}\rangle \langle\psi_{l_j,p_j}| \tag{6.37}$$

where $\zeta = \frac{z\Omega}{k}$. If we evolve an ancilla state, $|LG_{l_a,p_a}\rangle$, it will accumulate a dynamic phase of $\zeta(|l_a| + 2p_a + 1)$. This phase can then be removed from the output of $U(z)$, to produce a total unitary evolution governed by $e^{i\zeta H_{eff}}$ where the new effective Hamiltonian is

$$H_{eff} = \sum_i (|l_i| - |l_a| + 2p_i - 2p_a) |\psi_{l_i,p_i}\rangle \langle\psi_{l_i,p_i}|, \tag{6.38}$$

and the evolution of the state in the trap corresponds to the effecting time evolution operator, $U_{eff}(\zeta) \equiv e^{i\zeta H_{eff}}$. Any ancilla state, $|LG_{l_a,p_a}\rangle$, can result in a maximum of $|l_a| + 2p_a + 1$ states in s_{beam} with $\langle\psi_{l_i,p_i}| H_{eff} |\psi_{l_i,p_i}\rangle = 0$, $|l_a| + 2p_a + 2$ states with $\langle\psi_{l_i,p_i}| H_{eff} |\psi_{l_i,p_i}\rangle = 1$, and $|l_a| + 2p_a$ states with $\langle\psi_{l_i,p_i}| H_{eff} |\psi_{l_i,p_i}\rangle = -1$. Comparing to the Hamiltonians of the universal geometric gate set from Chapter 4, we see that every Hamiltonian in $G^{(D)}$ has exactly $D-1$ eigenstates with a corresponding eigenvalue of 0, one state with a corresponding eigenvalue of 1, and one state with a corresponding eigenvalue of -1. With this in mind, it is clear that choosing an ancilla state with $|l_a| + 2p_a \geq D-2$ allows s_{beam} to be constructed so that H_{eff} and $G^{(D)}_{(m,n)}$ have equivalent diagonal representations for any $D > 2$. If this is the case, then $U_{eff}(\pi)$ and $U^{(D)}_{(m,n)}$ will also have equivalent diagonal representations.

If the ancilla state has an energy exactly equal to $D-2$, then the set of zero-energy modes, $s_{beam,0}$ is

$$s_{beam,0} \equiv \{|\psi_{l,p}\rangle \ \mid p \in \mathbb{Z} \ \& \ p \in [0, \frac{1}{2}D - 1] \ \& \ l = \pm(D - 2p - 2)\} \tag{6.39}$$

Since only one state is required to have an energy of 1, we can pick $|\psi_{D-1,0}\rangle$ for simplicity. Likewise, pick $|\psi_{D-3,0}\rangle$ for the -1 energy state. s_{beam} is then the set given by $\{|\psi_{D-1,0}\rangle, |\psi_{D-3,0}\rangle\} \cup s_{beam,0}$. For notational convenience, the vectors in s_{beam} will be denoted $|\psi_{(i)}\rangle$, with the index i corresponding to the position of the vector in s_{beam} in the order given above. For example $|\psi_{(0)}\rangle = |\psi_{D-1,0}\rangle$, $|\psi_{(1)}\rangle = |\psi_{D-3,0}\rangle$, and so on.

Having established the set of LG modes contained in the beam, we can now consider the action of $U_{eff}(\zeta)$. If we let $|\psi_{(i)}\rangle = |G_{(m,n),i}\rangle$, given in Table 6.1, then the effective Hamiltonian in Eq. (6.38) becomes

$$H_{eff} = \omega_m |e\rangle \langle m| + \omega_n |e\rangle \langle n| + \omega_m^* |m\rangle \langle e| + \omega_n^* |n\rangle \langle e|. \tag{6.40}$$

Similarly, if the beam is evolved for a length of $\zeta = \pi$, then the effective evolution operator is

$$
\begin{aligned}
U_{eff} = & \left(|\omega_n|^2 - |\omega_m|^2\right)|m\rangle\langle m| - 2\omega_n\omega_m^*\,|m\rangle\langle n| - 2\omega_m\omega_n^*\,|n\rangle\langle m| + \\
& \left(|\omega_m|^2 - |\omega_n|^2\right)|n\rangle\langle n| + \left(\sum_{k\notin\{m,n\}}|k\rangle\langle k|\right) - |e\rangle\langle e|,
\end{aligned}
\tag{6.41}
$$

which is exactly equivalent to $U^{(D)}_{(m,n)}$ in the $\{|m\rangle, |n\rangle\}$ basis. This result shows that with the use of a clever change of basis, arbitrary unitary operations can be applied to the beam through a purely geometric evolution of the system. This process is very similar to a D-dimensional Zhu-Wang scheme. However, unlike the ZW scheme which generally relies on removing dynamic phases either during or after the evolution, this setup instead relies on evolving a state whose dynamic evolution is intrinsically suppressed.

Table 6.1 Eigenvectors of $G^{(D)}_{(m,n)}$ with corresponding eigenvalues.

Label	Eigenvector	Eigenvalue
$\|G_{(m,n),0}\rangle$	$\frac{1}{\sqrt{2}}\left(\omega_m^*\|m\rangle + \omega_n^*\|n\rangle + \|e\rangle\right)$	1
$\|G_{(m,n),1}\rangle$	$-\frac{1}{\sqrt{2}}\left(\omega_m^*\|m\rangle + \omega_n^*\|n\rangle - \|e\rangle\right)$	-1
$\|G_{(m,n),2}\rangle$	$\omega_n\|m\rangle - \omega_m\|n\rangle$	0
$\|G_{(m,n),i}\rangle$	$\|i\rangle \quad \forall \quad i \notin \{m,n,e\}$	0

Table 6.2 Eigenvectors of $U^{(D)}_{(m,n)}$ with corresponding eigenvalues.

Label	Eigenvector	Eigenvalue
$\|U_{(m,n),0}\rangle$	$\omega_m^*\|m\rangle + \omega_n^*\|n\rangle$	-1
$\|U_{(m,n),1}\rangle$	$\|e\rangle$	-1
$\|U_{(m,n),2}\rangle$	$\omega_n\|m\rangle - \omega_m\|n\rangle$	1
$\|U_{(m,n),i}\rangle$	$\|i\rangle \quad \forall \quad i \notin \{m,n,e\}$	1

6.5.1 Two-qubit encoding with $D = 4$

The two qubit case requires a total of five LG modes available to the system. We can choose any ancilla state with $|l| + 2p = D - 2$. Doing so will result in a zero energy subspace, $s_{beam,0}$, given by $\{|\psi_{2,0}\rangle, |\psi_{-2,0}\rangle, |\psi_{0,1}\rangle\}$ and a total LG mode space is spanned by the set s_{beam}, given by $\{|\psi_{3,0}\rangle, |\psi_{1,0}\rangle, |\psi_{2,0}\rangle, |\psi_{-2,0}\rangle, |\psi_{0,1}\rangle\}$. Note that if a particular experimental setup places restrictions on the available modes (for example, if the radial index, p, need be set to zero), then a higher energy ancilla state could be used and the mode space could be selected to fit those needs. We choose our basis so that $|\psi_{3,0}\rangle = |G_{(m,n),0}\rangle$, $|\psi_{1,0}\rangle = |G_{(m,n),1}\rangle$, $|\psi_{2,0}\rangle = |G_{(m,n),2}\rangle$, $|\psi_{-2,0}\rangle = |G_{(m,n),3}\rangle$, and $|\psi_{0,1}\rangle = |G_{(m,n),5}\rangle$. The qubit states will be represented by $|00\rangle = |0\rangle$, $|01\rangle = |1\rangle$, $|10\rangle = |2\rangle$, and $|11\rangle = |3\rangle$.

If we wanted to implement a CNOT gate, for example, we would use a single application of $U^{(D)}_{(2,3)}$ with $\omega_2 = \frac{1}{\sqrt{2}}$ and $\omega_3 = -\frac{1}{\sqrt{2}}$. Given an arbitrary computational input state, $|in\rangle = \alpha|0\rangle + \beta|1\rangle + \gamma|2\rangle + \delta|3\rangle$, the physical input state of the beam can be determined by inverting the basis transformation from $|\psi_{(i)}\rangle$ to $|G_{(m,n),0}\rangle$. The explicit basis transformation being done in this case is $|\psi_{(i)}\rangle = F_{j,i}\,|j\rangle$ where $F_{j,i}$ is

$$F = \begin{pmatrix} 0 & 0 & \frac{1}{2} & -\frac{1}{2} & \frac{1}{\sqrt{2}} \\ 0 & 0 & -\frac{1}{2} & \frac{1}{2} & \frac{1}{\sqrt{2}} \\ 0 & 0 & -\frac{1}{\sqrt{2}} & -\frac{1}{\sqrt{2}} & 0 \\ 1 & 0 & 0 & 0 & 0 \\ 0 & 1 & 0 & 0 & 0 \end{pmatrix} \tag{6.42}$$

(see Table 6.4 for a list of F matrices corresponding to all of the $U^{(4)}_{(m,n)}$ operators). Inverting the transformation, we get that $|i\rangle = F^{\dagger}_{j,i}\,|\psi_{(j)}\rangle$ where $F^{\dagger}$ is

$$F^{\dagger} = \begin{pmatrix} 0 & 0 & 0 & 1 & 0 \\ 0 & 0 & 0 & 0 & 1 \\ \frac{1}{2} & -\frac{1}{2} & -\frac{1}{\sqrt{2}} & 0 & 0 \\ -\frac{1}{2} & \frac{1}{2} & -\frac{2}{\sqrt{2}} & 0 & 0 \\ \frac{1}{\sqrt{2}} & \frac{1}{\sqrt{2}} & 0 & 0 & 0 \end{pmatrix}. \tag{6.43}$$

Using this transformation matrix, we see that $|0\rangle = |\psi_{-2,0}\rangle$, $|1\rangle = |\psi_{0,1}\rangle$, $|2\rangle = \frac{1}{2}\,|\psi_{3,0}\rangle - \frac{1}{2}\,|\psi_{1,0}\rangle - \frac{1}{\sqrt{2}}\,|\psi_{2,0}\rangle$, and $|3\rangle = -\frac{1}{2}\,|\psi_{3,0}\rangle + \frac{1}{2}\,|\psi_{1,0}\rangle - \frac{1}{\sqrt{2}}\,|\psi_{2,0}\rangle$. Thus, the input passed into the harmonic dielectric trap is a linear combination of LG modes given by

$$\begin{aligned} |LG_{in}\rangle = \alpha\left(|\psi_{-2,0}\rangle\right) + \beta\left(|\psi_{0,1}\rangle\right) + \gamma\left(\frac{1}{2}\,|\psi_{3,0}\rangle - \frac{1}{2}\,|\psi_{1,0}\rangle - \frac{1}{\sqrt{2}}\,|\psi_{2,0}\rangle\right) + \\ \delta\left(-\frac{1}{2}\,|\psi_{3,0}\rangle + \frac{1}{2}\,|\psi_{1,0}\rangle - \frac{1}{\sqrt{2}}\,|\psi_{2,0}\rangle\right). \end{aligned} \tag{6.44}$$

There are numerous methods to generate the input state. One simple and cost effective approach is to use a spatial light modulator (SLM) to produce the desired spatial modes. After evolving the beam through the trap for a length of $\zeta = \pi$, the resulting output state will be a new linear combination of LG modes, given by

$$|LG_{out}\rangle = \left(-\,|\psi_{3,0}\rangle\langle\psi_{3,0}| - |\psi_{1,0}\rangle\langle\psi_{1,0}| + |\psi_{2,0}\rangle\langle\psi_{2,0}| + |\psi_{-2,0}\rangle\langle\psi_{-2,0}| + |\psi_{0,1}\rangle\langle\psi_{0,1}|\right)|LG_{in}\rangle \tag{6.45}$$

$$= \frac{1}{2}\left(\delta - \gamma\right)|\psi_{3,0}\rangle + \frac{1}{2}\left(\gamma - \delta\right)|\psi_{1,0}\rangle - \frac{1}{\sqrt{2}}\left(\gamma + \delta\right)|\psi_{2,0}\rangle + \alpha\,|\psi_{-2,0}\rangle + \beta\,|\psi_{0,1}\rangle\,. \tag{6.46}$$

Finally, we convert the physical output back to the logical CNOT basis using the F transformation matrix. The simplest way to do this is manually applying the required transformation after measuring the physical output state. Once this is done, the final logical output is

$$
\begin{aligned}
|out\rangle =& \frac{1}{2}(\delta-\gamma)\left(\frac{1}{2}|2\rangle-\frac{1}{2}|3\rangle+\frac{1}{\sqrt{2}}|e\rangle\right)+\frac{1}{2}(\gamma-\delta)\left(-\frac{1}{2}|2\rangle+\frac{1}{2}|3\rangle+\frac{1}{\sqrt{2}}|e\rangle\right)- \\
& \frac{1}{\sqrt{2}}(\gamma+\delta)\left(-\frac{1}{\sqrt{2}}|2\rangle-\frac{1}{\sqrt{2}}|3\rangle\right)+\alpha|0\rangle+\beta|1\rangle \qquad (6.47) \\
=& \alpha|0\rangle+\beta|1\rangle+\delta|2\rangle+\gamma|3\rangle . \qquad (6.48)
\end{aligned}
$$

In the qubit representation, this operation has taken the input: $\alpha|00\rangle+\beta|01\rangle+\gamma|10\rangle+\delta|11\rangle$, to the output: $\alpha|00\rangle+\beta|01\rangle+\delta|10\rangle+\gamma|11\rangle$, thus performing a logical CNOT. In theory, arbitrary one and two qubit gates can be implemented on this platform, and Table 6.3 shows how to construct the universal gate set consisting of the CNOT gate, the PHASE gate, and the HADAMARD gate.

6.5.2 Physical Implementation and Unresolved Shortcomings

While the evolution within a harmonic dielectric trap is a rich environment to explore high dimensional holonomic gates, there are numerous gaps in the implementation that make it currently impractical as a means of achieving real world quantum computations. A good question to ask is: how, if at all, can a system like this be built in practice?

The first step is state preparation. Given the desired logical input and the F matrix of the operator being applied, the required physical input state can be determined. Once the desired state is known, it can be constructed using one of many known methods for LG mode preparation. One commonly used method utilizes a spatial light modulator (SLM) to display a holographic mask. When a $l=0, p=0$ mode is passed through the SLM, the hologram can be tuned to produce an arbitrary LG mode [32, 33]. Using this approach, we can generate the physical input associated with a particular gate.

With the input beam propagating in free space, the next step is to expose it to dielectric trapping. A simple approach is to use a graded index fiber with a quadratically varying index of refraction (as in Eq. (6.33)). Passing the beam through a fiber of length $\frac{k\pi}{\Omega}$ will apply the logic gate in the computational basis.

The final step of the operation is the part which challenges the practicality of the method. We must now convert the output of the gate back into the logical basis. If only one gate is to be applied, then the output can simply be measured and the result converted to the computational basis using post-processing on a classical machine. However, this requires the state to be fully measured, and in general this involves a measurement count that grows exponentially with qubit number [34]. Moreover, because the full state must be classically stored and manipulated to transform the state in this manner, it suffers from the limitations of classical computers.

The alternative is to carry out the transformation using physical mode converters. Unfortunately, traditional mode converters are only capable of converting between modes of equal mode order [35]. This is equivalent to restricting the allowed transformations to an equal energy subspace of the beam space, which is not sufficient for our needs. That said, it may be possible to split the LG modes into separate paths using a programmable mode sorter [36]. After splitting the modes into separate beams, traditional linear optical methods (such as the Reck scheme or KLM protocol) could carry out the transformation, after which the modes would be recombined.

Needless to say, this is not yet a practical means of achieving quantum logic. In fact, in the latter method, the final operations are not even holonomic because the traditional linear optical processing schemes are not guaranteed to meet the necessary requirements.

Table 6.3 $U^{(4)}_{(m,n)}$ operators corresponding to the universal two qubit gate set, {CNOT, Phase (P), HADAMARD (H)}.

Gate	$U^{(4)}_{(m,n)}(\omega_m, \omega_n)$ Sequence
$\mathrm{CNOT}_{0,1}$	$U^{(4)}_{(2,3)}\left(\frac{1}{\sqrt{2}}, -\frac{1}{\sqrt{2}}\right)$
$\mathrm{CNOT}_{1,0}$	$U^{(4)}_{(1,3)}\left(\frac{1}{\sqrt{2}}, -\frac{1}{\sqrt{2}}\right)$
H⊗I	$U^{(4)}_{(1,3)}\left(\sin\left(\frac{\pi}{8}\right), -\cos\left(\frac{\pi}{8}\right)\right) U^{(4)}_{(0,2)}\left(\sin\left(\frac{\pi}{8}\right), -\cos\left(\frac{\pi}{8}\right)\right)$
I⊗H	$U^{(4)}_{(0,1)}\left(\sin\left(\frac{\pi}{8}\right), -\cos\left(\frac{\pi}{8}\right)\right) U^{(4)}_{(2,3)}\left(\sin\left(\frac{\pi}{8}\right), -\cos\left(\frac{\pi}{8}\right)\right)$
P⊗I	$U^{(4)}_{(1,3)}\left(\frac{e^{-\frac{i\phi}{2}}}{\sqrt{2}}, -\frac{e^{\frac{i\phi}{2}}}{\sqrt{2}}\right) U^{(4)}_{(1,3)}\left(\frac{1}{\sqrt{2}}, -\frac{1}{\sqrt{2}}\right) U^{(4)}_{(0,3)}\left(\frac{e^{-\frac{i\phi}{2}}}{\sqrt{2}}, -\frac{e^{\frac{i\phi}{2}}}{\sqrt{2}}\right) \times$ $\mathrm{U}^{(4)}_{(0,3)}\left(\frac{1}{\sqrt{2}}, -\frac{1}{\sqrt{2}}\right) U^{(4)}_{(2,3)}\left(\frac{e^{\frac{i\phi}{2}}}{\sqrt{2}}, -\frac{e^{-\frac{i\phi}{2}}}{\sqrt{2}}\right) U^{(4)}_{(2,3)}\left(\frac{1}{\sqrt{2}}, -\frac{1}{\sqrt{2}}\right)$
I⊗P	$U^{(4)}_{(0,1)}\left(\frac{e^{-\frac{i\phi}{2}}}{\sqrt{2}}, -\frac{e^{\frac{i\phi}{2}}}{\sqrt{2}}\right) U^{(4)}_{(0,1)}\left(\frac{1}{\sqrt{2}}, -\frac{1}{\sqrt{2}}\right) U^{(4)}_{(2,3)}\left(\frac{e^{-\frac{i\phi}{2}}}{\sqrt{2}}, -\frac{e^{\frac{i\phi}{2}}}{\sqrt{2}}\right) U^{(4)}_{(2,3)}\left(\frac{1}{\sqrt{2}}, -\frac{1}{\sqrt{2}}\right)$

Table 6.4 F matrices corresponding to the $U^{(4)}_{(m,n)}$ operators.

Target Operator	F Matrix
$U^{(4)}_{(0,1)}(\omega_1, \omega_2)$	$\begin{pmatrix} \frac{(\omega_0)^*}{\sqrt{2}} & \frac{(\omega_1)^*}{\sqrt{2}} & 0 & 0 & \frac{1}{\sqrt{2}} \\ -\frac{(\omega_0)^*}{\sqrt{2}} & -\frac{(\omega_1)^*}{\sqrt{2}} & 0 & 0 & \frac{1}{\sqrt{2}} \\ \omega_1 & -\omega_0 & 0 & 0 & 0 \\ 0 & 0 & 1 & 0 & 0 \\ 0 & 0 & 0 & 1 & 0 \end{pmatrix}$
$U^{(4)}_{(0,2)}(\omega_1, \omega_2)$	$\begin{pmatrix} \frac{(\omega_0)^*}{\sqrt{2}} & 0 & \frac{(\omega_2)^*}{\sqrt{2}} & 0 & \frac{1}{\sqrt{2}} \\ -\frac{(\omega_0)^*}{\sqrt{2}} & 0 & -\frac{(\omega_2)^*}{\sqrt{2}} & 0 & \frac{1}{\sqrt{2}} \\ \omega_2 & 0 & -\omega_0 & 0 & 0 \\ 0 & 1 & 0 & 0 & 0 \\ 0 & 0 & 0 & 1 & 0 \end{pmatrix}$
$U^{(4)}_{(0,3)}(\omega_1, \omega_2)$	$\begin{pmatrix} \frac{(\omega_0)^*}{\sqrt{2}} & 0 & 0 & \frac{(\omega_3)^*}{\sqrt{2}} & \frac{1}{\sqrt{2}} \\ -\frac{(\omega_0)^*}{\sqrt{2}} & 0 & 0 & -\frac{(\omega_3)^*}{\sqrt{2}} & \frac{1}{\sqrt{2}} \\ \omega_3 & 0 & 0 & -\omega_0 & 0 \\ 0 & 1 & 0 & 0 & 0 \\ 0 & 0 & 1 & 0 & 0 \end{pmatrix}$
$U^{(4)}_{(1,2)}(\omega_1, \omega_2)$	$\begin{pmatrix} 0 & \frac{(\omega_1)^*}{\sqrt{2}} & \frac{(\omega_2)^*}{\sqrt{2}} & 0 & \frac{1}{\sqrt{2}} \\ 0 & -\frac{(\omega_1)^*}{\sqrt{2}} & -\frac{(\omega_2)^*}{\sqrt{2}} & 0 & \frac{1}{\sqrt{2}} \\ 0 & \omega_2 & -\omega_1 & 0 & 0 \\ 1 & 0 & 0 & 0 & 0 \\ 0 & 0 & 0 & 1 & 0 \end{pmatrix}$
$U^{(4)}_{(1,3)}(\omega_1, \omega_2)$	$\begin{pmatrix} 0 & \frac{(\omega_1)^*}{\sqrt{2}} & 0 & \frac{(\omega_3)^*}{\sqrt{2}} & \frac{1}{\sqrt{2}} \\ 0 & -\frac{(\omega_1)^*}{\sqrt{2}} & 0 & -\frac{(\omega_3)^*}{\sqrt{2}} & \frac{1}{\sqrt{2}} \\ 0 & \omega_3 & 0 & -\omega_1 & 0 \\ 1 & 0 & 0 & 0 & 0 \\ 0 & 0 & 1 & 0 & 0 \end{pmatrix}$
$U^{(4)}_{(2,3)}(\omega_1, \omega_2)$	$\begin{pmatrix} 0 & 0 & \frac{(\omega_2)^*}{\sqrt{2}} & \frac{(\omega_3)^*}{\sqrt{2}} & \frac{1}{\sqrt{2}} \\ 0 & 0 & -\frac{(\omega_2)^*}{\sqrt{2}} & -\frac{(\omega_3)^*}{\sqrt{2}} & \frac{1}{\sqrt{2}} \\ 0 & 0 & \omega_3 & -\omega_2 & 0 \\ 1 & 0 & 0 & 0 & 0 \\ 0 & 1 & 0 & 0 & 0 \end{pmatrix}$

CHAPTER 7
CONCLUSIONS AND FUTURE WORK

In this thesis, we sought to answer the question: Can trapped optical modes be used to carry out universal holonomic quantum computation? Answering this required the study and consideration of three different topics: quantum computing, geometric phases, and optics.

First, a general background for quantum computing was established. This involved motivating the need for quantum computers, and gave a basic mathematical formulation governing the analysis of quantum information systems. Next, the concepts of geometric phases and holonomies were introduced. Geometric phase was first presented in the context of adiabatic evolution, but was extended to include more general cases. It was also shown how certain conditions can give rise to non-Abelian geometric holonomies.

Given the background of quantum computing and geometric phase, two existing platform for purely holonomic quantum computation were studied. The first used non-Abelian holonomies on a three-level trapped ion to enable universal computing. The primary structure of this example was then generalized to allow for scaling into an arbitrarily large vector space. The second technique, called the ZW scheme, demonstrated that Abelian geometric phases can also be used to carry out holonomic quantum computations so long as a suitable basis transformation can be performed.

Finally, the final piece of necessary background information was discussed: optics. We first presented and discussed LOQC, and gave an overview of two existing strategies to process quantum information using linear optical elements. Next, we showed how Abelian geometric phases generate in optical systems in the same way they do in quantum systems. Lastly, we showed that under the correct conditions, a classical beam of light can be treated as a quantum particle in two-spatial dimensions, with the optical Z-axis corresponding to the temporal axis of the quantum system using the paraxial equation.

Having all of these components well established, we proposed a novel quantum computing method which combines elements of all of these fields. This new scheme uses the paraxial evolution of Laguerre-Gaussian modes in a harmonic dielectric trap to perform holonomic quantum gates. This is done by transforming to a logical basis in which the system Hamiltonian has a trivial effect on the evolution, thus making it purely holonomic.

Through the analysis of these key topics and the proposal of a new holonomic quantum computing scheme using optical modes, we have established an answer to the thesis question: trapped optical modes can, in theory, be used to carry out universal holonomic quantum computation. However, more work is required before the strategy can be used in practice.

Unlike the ZW scheme, where basis transformations can easily be made by changing free parameters of the system, the LG method does not allow for a simple change of basis to be applied. In the current implementation, the only freedom to select the desired gate is in the initial state preparation. To make the method more practical, improvements must be made to allow for on-the-fly basis transformations.

One potential direction for future work is to consider how to make the trap strength, Ω, vary as a function of the azimuthal and radial indices. For example, consider a dielectric trap with a trap strength that varies according to

$$\Omega_{l,p} = \Omega_0 - \alpha l \tag{7.1}$$

for some constant α. Then, a single-qubit Hilbert space could be constructed using the $|\psi_{4,0}\rangle$, $|\psi_{0,2}\rangle$, and $|\psi_{2,1}\rangle$ eigenmodes. All of these modes have an energy given by $\epsilon_{l,p} = \frac{5\Omega_{l,p}}{k}$. If we choose the $|\psi_{2,1}\rangle$ mode to also be the ancilla mode, then the effective Hamiltonian becomes

$$H_{eff} = \frac{2\alpha}{5k} \left(|\psi_{0,2}\rangle \langle\psi_{0,2}| - |\psi_{4,0}\rangle \langle\psi_{4,0}| \right), \tag{7.2}$$

which matches the diagonal form of $G^{(2)}_{(0,1)}$. The key distinction between this construction and the proposed setup is that these modes are all of the same mode order. Thus, traditional mode converters can be used to rotate the frame in between sequential operations [35]. By using mode converters to enact the required basis transformations, Eq(7.2) can be used to generate a universal single qubit gate.

We note that this work fits into a larger field of study which deals with quantum computing using Laguerre-Gaussian Beams. There are two approaches commonly considered when storing quantum information in LG beams: the Orbital Angular Momentum (OAM) Approach, and the Multimode Fiber (MMF) Approach [37]. Both of these strategies focus on the use of optical elements to generate unitary operations on a superposition of LG modes. However, the OAM approach is based on the use of linear optical elements such as lenses, prisms, and mirrors, while the MMF approach relies on the use of optic fibers that support large numbers of optical modes. Our technique is an example of the MMF approach, using fibers that bave a parabolic, radial dielectric profile.

There has and continues to be tremendous progress in both of these areas. For example, both the OAM [38, 39] and the MMF [37, 40] frameworks offer strategies to implement universal sets of logic gates on optical modes. However, neither have been extended to the regime of purely geometric evolutions. This work has helped expand the MMF approach to allow for such holonomic gates to be implemented.

REFERENCES

[1] Georges Ifrah and E. F. Harding. *The Universal History of Computing: From the Abacus to the Quantum Computer*. John Wiley Sons, Inc., USA, 1st edition, 2001. ISBN 0471441473.

[2] Kyriakos Efstathiou and Marianna Efstathiou. Celestial Gearbox. *Mechanical Engineering*, 140(09): 31–35, 09 2018. ISSN 0025-6501. doi: 10.1115/1.2018-SEP1. URL https://doi.org/10.1115/1.2018-SEP1.

[3] Erik Gregersen. Analog computer, Oct 2021. URL https://www.britannica.com/technology/analog-computer.

[4] F. Rosenblatt. The perceptron: A probabilistic model for information storage and organization in the brain. *Psychological Review*, 65(6):386–408, Nov 1958. doi: 10.1037/h0042519.

[5] Kiril Boyanov. John vincent atanasoff: the inventor of the first electronic digital computing. 06 2003. doi: 10.1145/973620.973621.

[6] M. Karnaugh. The map method for synthesis of combinational logic circuits. *Transactions of the American Institute of Electrical Engineers, Part I: Communication and Electronics*, 72(5):593–599, 1953. doi: 10.1109/TCE.1953.6371932.

[7] Jack D. Hidary. *Quantum Computing: An Applied Approach*. Springer, Cham, 2019. ISBN 978-3-030-23921-3. doi: https://doi.org/10.1007/978-3-030-23922-0.

[8] Arjen Lenstra, Hendrik Lenstra, Mark Manasse, and John Pollard. The number field sieve. pages 564–572, 01 1990. doi: 10.1145/100216.100295.

[9] Peter W. Shor. Polynomial-time algorithms for prime factorization and discrete logarithms on a quantum computer. *SIAM Journal on Computing*, 26(5):1484–1509, 1997. doi: 10.1137/S0097539795293172. URL https://doi.org/10.1137/S0097539795293172.

[10] Eliot Kapit. *Quantum Engineering (A Conversational Guide to the Secret Language of the World*. In preparation, 2020.

[11] Dorit Aharonov. A simple proof that toffoli and hadamard are quantum universal, 2003. URL https://doi.org/10.48550/arXiv.quant-ph/0301040.

[12] Francisco De Zela. The pancharatnam-berry phase: Theoretical and experimental aspects. In Mohammad Reza Pahlavani, editor, *Theoretical Concepts of Quantum Mechanics*, chapter 14. IntechOpen, Rijeka, 2012. doi: 10.5772/34882. URL https://doi.org/10.5772/34882.

[13] Y. Aharonov and J. Anandan. Phase change during a cyclic quantum evolution. *Phys. Rev. Lett.*, 58: 1593–1596, Apr 1987. doi: 10.1103/PhysRevLett.58.1593. URL https://link.aps.org/doi/10.1103/PhysRevLett.58.1593.

[14] Joseph Samuel and Rajendra Bhandari. General setting for berry's phase. *Phys. Rev. Lett.*, 60: 2339–2342, Jun 1988. doi: 10.1103/PhysRevLett.60.2339. URL https://link.aps.org/doi/10.1103/PhysRevLett.60.2339.

[15] Frank Wilczek and A. Zee. Appearance of gauge structure in simple dynamical systems. *Phys. Rev. Lett.*, 52:2111–2114, Jun 1984. doi: 10.1103/PhysRevLett.52.2111. URL https://link.aps.org/doi/10.1103/PhysRevLett.52.2111.

[16] J. Anandan. Non-adiabatic non-abelian geometric phase. *Physics Letters A*, 133(4):171–175, 1988. ISSN 0375-9601. doi: https://doi.org/10.1016/0375-9601(88)91010-9. URL https://www.sciencedirect.com/science/article/pii/0375960188910109.

[17] Arno Bohm. *The geometric phase in quantum systems : foundations, mathematical concepts, and applications in molecular and condensed matter physics*. Springer, Berlin New York, 2003. ISBN 978-3-642-05504-1.

[18] Todd Rowland. Holonomy group. from mathworld—a wolfram web resource, created by eric w. weisstein. URL http://mathworld.wolfram.com/HolonomyGroup.html.

[19] Eliot Kapit, John Chalker, and Steven Simon. Passive correction of quantum logical errors in a driven, dissipative system: A blueprint for an analog quantum code fabric. *Physical Review A*, 91, 08 2014. doi: 10.1103/PhysRevA.91.062324.

[20] Jiannis K. Pachos. *Introduction to Topological Quantum Computation*. Cambridge University Press, 2012. doi: 10.1017/CBO9780511792908.

[21] Austin G. Fowler, Matteo Mariantoni, John M. Martinis, and Andrew N. Cleland. Surface codes: Towards practical large-scale quantum computation. *Physical Review A*, 86(3), Sep 2012. ISSN 1094-1622. doi: 10.1103/physreva.86.032324. URL http://dx.doi.org/10.1103/PhysRevA.86.032324.

[22] John M Martinis. Saving superconducting quantum processors from qubit decay and correlated errors generated by gamma and cosmic rays. *arXiv*, quant-ph/2012.06137v3, May 2021. URL https://doi.org/10.48550/arXiv.2012.06137.

[23] Matt McEwen, Lara Faoro, Kunal Arya, Andrew Dunsworth, Trent Huang, Seon Kim, Brian Burkett, Austin Fowler, Frank Arute, Joseph C. Bardin, Andreas Bengtsson, Alexander Bilmes, Bob B. Buckley, Nicholas Bushnell, Zijun Chen, Roberto Collins, Sean Demura, Alan R. Derk, Catherine Erickson, Marissa Giustina, Sean D. Harrington, Sabrina Hong, Evan Jeffrey, Julian Kelly, Paul V. Klimov, Fedor Kostritsa, Pavel Laptev, Aditya Locharla, Xiao Mi, Kevin C. Miao, Shirin Montazeri, Josh Mutus, Ofer Naaman, Matthew Neeley, Charles Neill, Alex Opremcak, Chris Quintana, Nicholas Redd, Pedram Roushan, Daniel Sank, Kevin J. Satzinger, Vladimir Shvarts, Theodore White, Z. Jamie Yao, Ping Yeh, Juhwan Yoo, Yu Chen, Vadim Smelyanskiy, John M. Martinis, Hartmut Neven, Anthony Megrant, Lev Ioffe, and Rami Barends. Resolving catastrophic error bursts from cosmic rays in large arrays of superconducting qubits. *Nature Physics*, 18(1):107–111, Jan 2022. ISSN 1745-2481. doi: 10.1038/s41567-021-01432-8. URL https://doi.org/10.1038/s41567-021-01432-8.

[24] Erik Sjöqvist, D M Tong, L Mauritz Andersson, Björn Hessmo, Markus Johansson, and Kuldip Singh. Non-adiabatic holonomic quantum computation. *New Journal of Physics*, 14(10):103035, oct 2012. doi: 10.1088/1367-2630/14/10/103035. URL https://doi.org/10.1088/1367-2630/14/10/103035.

[25] Shi-Liang Zhu and Z. D. Wang. Implementation of universal quantum gates based on nonadiabatic geometric phases. *Physical Review Letters*, 89(9), Aug 2002. ISSN 1079-7114. doi: 10.1103/physrevlett.89.097902. URL http://dx.doi.org/10.1103/PhysRevLett.89.097902.

[26] C. R. Myers and R. Laflamme. Linear optics quantum computation: an overview. *arXiv*, quant-ph/0512104, 2005. URL https://doi.org/10.48550/arXiv.quant-ph/0512104.

[27] Michael Chapman and Todd Heinrichs. *Cavity QED Approaches to Quantum Information Processing and Quantum Computing*. Advanced Research and Development Activity, 2004. URL https://qist.lanl.gov/pdfs/cavity_qed.pdf.

[28] Michael Reck, Anton Zeilinger, Herbert J. Bernstein, and Philip Bertani. Experimental realization of any discrete unitary operator. *Phys. Rev. Lett.*, 73:58–61, Jul 1994. doi: 10.1103/PhysRevLett.73.58. URL https://link.aps.org/doi/10.1103/PhysRevLett.73.58.

[29] Nicholas C. Harris, Jacques Carolan, Darius Bunandar, Mihika Prabhu, Michael Hochberg, Tom Baehr-Jones, Michael L. Fanto, A. Matthew Smith, Christopher C. Tison, Paul M. Alsing, and Dirk Englund. Linear programmable nanophotonic processors. *Optica*, 5(12):1623–1631, Dec 2018. doi: 10.1364/OPTICA.5.001623. URL http://opg.optica.org/optica/abstract.cfm?URI=optica-5-12-1623.

[30] Timothy M. Pritchett and A. David Trubatch. A differential formulation of diffraction theory for the undergraduate optics course. *American Journal of Physics*, 72(8):1026–1034, 2004. doi: 10.1119/1.1758226. URL https://doi.org/10.1119/1.1758226.

[31] S. Cruz y Cruz, Z. Gress, P. Jiménez-Macías, and O. Rosas-Ortiz. Laguerre–gaussian wave propagation in parabolic media. In Piotr Kielanowski, Anatol Odzijewicz, and Emma Previato, editors, *Geometric Methods in Physics XXXVIII*, pages 117–128, Cham, 2020. Springer International Publishing.

[32] Yoshiyuki Ohtake, Taro Ando, Naoya Matsumoto, Takashi Inoue, Norihiro Fukuchi, Haruyasu Itoh, Naohisa Mukohzaka, and Tsutomu Hara. High-quality generation of higher-order Laguerre-Gaussian beams using liquid crystal on silicon spatial light modulator. In David L. Andrews, Enrique J. Galvez, and Gerard Nienhuis, editors, *Complex Light and Optical Forces II*, volume 6905, pages 50 – 58. International Society for Optics and Photonics, SPIE, 2008. doi: 10.1117/12.762538. URL https://doi.org/10.1117/12.762538.

[33] Frédéric Bouchard, Natalia Herrera Valencia, Florian Brandt, Robert Fickler, Marcus Huber, and Mehul Malik. Measuring azimuthal and radial modes of photons. *Optics Express*, 26(24):31925, Nov 2018. ISSN 1094-4087. doi: 10.1364/oe.26.031925. URL http://dx.doi.org/10.1364/OE.26.031925.

[34] Joseph B. Altepeter, Daniel F.V. James, and Paul G. Kwiat. 4 qubit quantum state tomography. In *Quantum State Estimation*, pages 113–145. Springer Berlin Heidelberg, August 2004. doi: 10.1007/978-3-540-44481-7_4. URL https://doi.org/10.1007/978-3-540-44481-7_4.

[35] L. Allen, J. Courtial, and M. J. Padgett. Matrix formulation for the propagation of light beams with orbital and spin angular momenta. *Phys. Rev. E*, 60:7497–7503, Dec 1999. doi: 10.1103/PhysRevE.60.7497. URL https://link.aps.org/doi/10.1103/PhysRevE.60.7497.

[36] David A. B. Miller. Self-configuring universal linear optical component. *Photon. Res.*, 1(1):1–15, Jun 2013. doi: 10.1364/PRJ.1.000001. URL http://opg.optica.org/prj/abstract.cfm?URI=prj-1-1-1.

[37] Yu Wang, Václav Potoček, Stephen M. Barnett, and Xue Feng. Programmable holographic technique for implementing unitary and nonunitary transformations. *Phys. Rev. A*, 95:033827, Mar 2017. doi: 10.1103/PhysRevA.95.033827. URL https://link.aps.org/doi/10.1103/PhysRevA.95.033827.

[38] Juan Carlos García-Escartín and Pedro Chamorro-Posada. Universal quantum computation with the orbital angular momentum of a single photon. *Journal of Optics*, 13(6):064022, apr 2011. doi: 10.1088/2040-8978/13/6/064022. URL https://doi.org/10.1088/2040-8978/13/6/064022.

[39] Frédéric Bouchard, Natalia Herrera Valencia, Florian Brandt, Robert Fickler, Marcus Huber, and Mehul Malik. Measuring azimuthal and radial modes of photons. *Opt. Express*, 26(24):31925–31941, Nov 2018. doi: 10.1364/OE.26.031925. URL http://opg.optica.org/oe/abstract.cfm?URI=oe-26-24-31925.

[40] Ohad Lib, Kfir Sulimany, and Yaron Bromberg. Reconfigurable synthesizer for quantum information processing of high-dimensional entangled photons, 2021. URL https://arxiv.org/abs/2108.02258.